H2A.Z facilitates Sox2-nucleosome interaction by promoting DNA and histone H3 tail mobility

Helen K. Moos[1], Rutika Patel[2,3], Sophie K. Flaherty[1], Sharon M. Loverde[2,3,4,5] and Evgenia N. Nikolova[1]

[1]T.C. Jenkins Department of Biophysics, Johns Hopkins University, Baltimore, MD, 21218

[2]Ph.D. Program in Biochemistry, The Graduate Center of the City University of New York, New York, NY, 10016

[3]Department of Chemistry, College of Staten Island, The City University of New York, 2800 Victory Boulevard, Staten Island, New York, 10314, United States.

[4]Ph.D. Program in Chemistry, The Graduate Center of the City University of New York, New York, NY, 10016

[5]Ph.D. Program in Physics, The Graduate Center of the City University of New York, New York, NY, 10016

Correspondence to Evgenia N. Nikolova: *enikolova@jhu.edu*

Abstract

Epigenetic regulation of eukaryotic chromatin structure and function can be modulated by histone variants and post-translational modifications. The conserved variant H2A.Z has been functionally linked to pioneer factors Sox2 and Oct4 that open chromatin and initiate cell fate-specific expression programs. However, the molecular basis for their interaction remains unknown. Using biochemistry, nuclear magnetic resonance (NMR) spectroscopy and molecular dynamics (MD) simulations, we examine the role of H2A.Z nucleosome dynamics in pioneer factor binding. We find that H2A.Z facilitates Sox2 and Oct4 binding at distinct locations in 601 nucleosomes. We further link this to increased DNA accessibility and perturbed dynamics of the H3 N-terminal tail, which we show competes with Sox2 for DNA binding. Our simulations validate a coupling between H2A.Z-mediated DNA unwrapping and altered H3 N-tail conformations with fewer contacts to DNA and the H2A.Z C-terminal tail. This destabilizing effect of H2A.Z is DNA sequence dependent and enhanced with the less stable Lin28B nucleosome. Collectively, our findings suggest that H2A.Z promotes pioneer factor binding by increasing access to DNA and reducing competition with H3 tails. This could have broader implications for how epigenetic marks or oncogenic mutations tune pioneer factor engagement with chromatin and thus affect its structure and recognition.

Keywords

H2A.Z variant, pioneer factors, nucleosome dynamics, histone tail mobility, DNA accessibility

Introduction

Epigenetic changes such as post-translational modifications (PTMs) and histone variants play critical roles in regulating the structure and function of chromatin.[1, 2] H2A.Z is a highly conserved histone variant that is crucial for transcriptional regulation, genome integrity, DNA damage repair, and chromosome segregation[3-6]. H2A.Z is required for embryonic stem cell renewal and differentiation[7], and its dysregulation has been linked to embryonic abnormalities and cancer.[6, 8] Despite extensive studies, how H2A.Z regulates chromatin structure remains to be characterized on a molecular level.

Within the genome, H2A.Z is enriched at regulatory regions of both active and inactive genes[9] and, depending on its location, can either activate or repress transcription.[10-12] At actively transcribing genes, this variant is frequently acetylated[13] and its occupancy strongly correlates with epigenetic marks such as H3K4 methylation.[14, 15] Importantly, H2A.Z is known to affect chromatin structure, reducing nucleosome occupancy and increasing chromatin accessibility *in vivo.*[16-18] H2A.Z has been functionally linked to pioneer transcription factors[7, 19-22] that promote chromatin opening and remodeling during embryonic stem cell (ESC) renewal and differentiation.[23, 24] H2A.Z marks motifs and nucleosome-occupied regions of the pioneer factors Sox2 and Oct4 and an H2A.Z knockdown compromises Oct4 binding to its target genes.[7, 21, 25 25, 26] H2A.Z can also cooperate with Sox2 in recruiting the repressive complex PRC2.[25] These studies suggest an important role of H2A.Z in mediating chromatin structure and its interaction with regulatory proteins that orchestrate cell fate.

Increases in nucleosome dynamics such as the spontaneous “breathing” or unwrapping of DNA have been shown to increase the binding of transcription factors *in vitro*.[27, 28] MD simulations have established that DNA unwrapping is tightly linked to the dynamics of the histone N- and C-terminal tails protruding out of the nucleosome core.[29-31] As shown by NMR and computational studies, histone tails are highly flexible and interact dynamically with nucleosomal and linker DNA, which can inhibit the binding of regulatory proteins.[29-35] Interactions of the H3 N-terminal and H2A C-terminal tail at super-helical locations (SHLs) near entry/exit DNA are particularly important as those regions are a primary target for transcription factors.[36-38] Moreover, experiments and theoretical models suggest that histone tail proteolytic cleavage, charge-altering PTMs, and oncogenic mutations, often found in H3 and H2A tails,[39-41] further modulate interactions of chromatin with regulatory factors.[1, 29, 35, 42] Thus, pioneer factors can exploit differences in nucleosome dynamics for efficient targeting, which could facilitate chromatin opening and enable recruitment of other factors.

Structural and biochemical studies support the role of H2A.Z in chromatin destabilization. Incorporation of H2A.Z in nucleosomes leads to lower thermal stability and increased DNA unwrapping compared to canonical systems.[43, 44] The distinct H2A.Z N- and C-terminal regions, which contain fewer positively charged residues, have been implicated in this process.[45] The Cryo-electron microscopy (Cryo-EM) structure of an H2A.Z nucleosome containing the Widom 601 positioning sequence shows enhanced asymmetric unwrapping and potential weaker contacts of the H2A.Z C-terminal region with DNA and histone H3.[44] However, the flexible tails of H2A.Z and other histones are not visualized, preventing insight into their conformation, dynamics, and interactions. Molecular dynamics (MD) simulations corroborate these structural findings and begin to fill in the mechanistic gaps.[46, 47] They have identified increased histone plasticity and a coupling between DNA unwrapping and loss of H2A.Z C-terminal tail-DNA contacts in nucleosomes.[46, 47] While some insights into the dynamics of H2A.Z nucleosomes exist, little is known about other histone tail perturbations and how they impact pioneer factor interactions.

H2A.Z-associated Sox2 and Oct4 are key pioneer factors that engage with silent chromatin in ESCs and promote transcriptional programs to control cell-fate decisions.[24, 48] These pioneer factors are also essential for somatic cell reprogramming into induced pluripotent stem cells (iPSC).[49, 50] Sox2 and Oct4

can bind synergistically and interact on adjacent or closely spaced motifs *in vitro* [51, 52] and co-localize on target genes *in vivo*.[49, 53] Sox2 contains a partially disordered high mobility group (HMG) box DNA binding domain (DBD) that adopts a folded conformation when bound to the DNA minor groove, and severely bends and unwinds the DNA helix.[54, 55] The binding of Sox2 to the nucleosome and the extent of DNA deformation is dictated by multiple factors, including the intrinsic flexibility of Sox2, as well as the DNA sequence, accessibility, and mobility.[56-59] Biochemical and high-resolution studies have established that Sox2 primarily targets solvent-exposed sites on nucleosomes, with a strong preference for SHL5 and lower preference for SHL2 and SHL6.[57-59] Oct4 recognizes DNA using a bi-partite DBD containing a POU-specific domain (POU_S) and a POU-homeodomain (POU_{HD}) joined by a flexible linker, where the two domains interact with opposite faces of the DNA major groove.[54, 55] Oct4 favors entry/exit sites with an accessible half-motif (for POU_S or POU_{HD}), where DNA unwrapping can expose the other half-motif, or linker DNA, where binding is modulated by interactions with the H3 and H4 N-terminal tails.[58, 60-62] In less stable nucleosomes that exhibit greater DNA mobility, such as Lin28B, Oct4 can gain access to more internal sites.[60, 61] Since DNA dynamics can dictate the interaction of pioneer factors with nucleosomes, it is important to elucidate the role of H2A.Z and other epigenetic changes in modulating these interactions.

Here, we investigate the underlying mechanisms of how H2A.Z affects Sox2 and Oct4 association with nucleosomes. Using NMR spectroscopy, MD simulations, and biochemistry, combined with targeted mutagenesis, we examine the relationship between DNA mobility, histone tail dynamics, and pioneer factor binding. We find that H2A.Z can enhance the interaction of Sox2 and Oct4 with end-positioned (SHL6) and internal sites (SHL2 for Sox2), where DNA unwrapping is increased and histone H3 tail dynamics are perturbed. Additionally, we show that Sox2 displaces the H3 N-terminal tail, and more so with H2A.Z, when binding to those sites. MD simulations further reveal that more extensive DNA unwrapping with H2A.Z correlates with more disordered H3 tail conformations and reduced contacts between the H3 tail, flanking DNA, and the H2A.Z C-terminal tail. Together, our findings suggest that H2A.Z can guide Sox2 and Oct4 interaction with nucleosomes by promoting DNA and H3 tail mobility.

Materials and Methods

Sox2 and Oct4 preparation

The human Sox2 DBD (39-118), and Oct4 DBD (133-296) were designed as described previously.[59] An Oct4 “CtoS” mutant was created via standard mutagenesis where all cysteine residues were substituted with serine to create a stabilized construct and reduce protein aggregation. DNA binding was tested and found to be equivalent to the wild-type protein. Proteins were expressed in BL21(DE3) cells in TB media. Cells were grown with shaking at 37 °C until OD_{600} ~0.6, induced with 0.5 mM IPTG, then grown for 4 h at 37 °C for Sox2, and 16-18 h at 18 °C for Oct4. Cells were harvested by centrifugation at 3600 RPM for 20 min, and pellets were stored at -20 °C. Purification was done via a two-step Ni^2+ affinity chromatography on an AKTA FPLC system (Cytiva), as described previously,[59] where the His-tag was cleaved using an in-house His-tagged 3C protease.

Histone preparation

Human H2A.Z in pET21a was gifted by Prof. Carl Wu (JHU). *Xenopus laevis* (XL) histones H2A, H2B, H3, and H4 in pET3a were a gift from Prof. Gregory Bowman (JHU). Mutant constructs were prepared using standard mutagenesis. XL histone plasmids and $H2A^{C\text{-}H2A.Z}$ mutant were transformed into BL21(DE3) pLysS for expression in 2XTY media (unlabeled) or M9 media (isotopic labelling), except for ^{15}N-labeled H4 that was expressed in BL21(DE3) cells. Human H2A.Z and mutant constructs were expressed in BL21(DE3) cells. For ^{15}N or ^{15}N,^{13}C labeling, M9 media was supplemented with 1 g $^{15}NH_4Cl$ and 2 g ^{13}C-glucose (CIL). For XL H2A, H2B, H3, and human H2A.Z, cell pellets were purified on a 20 ml Q-SP HiTrap HP column (Cytiva, 2x5 ml Q on top of 2x5 ml SP), using a Sodium Acetate-

Urea buffer, as previously described.[59] Histone H4 was prepared from inclusion bodies, followed by a desalting column (HiPrep 26/10 (GE)) and a 2X Q-SP column (Cytiva), as previously described.[59, 63]

DNA preparation

DNA for mouse Fgf4 (CTTTGTTTGGATGCTAAT) and Nanog (CATTGTAATGCAAAA) composite motifs were inserted via standard mutagenesis within the Widom 601 sequence in pGEM-3z/601 plasmid (gift from Prof. Gregory Bowman, JHU), which we modified on one end to remove a strong non-cognate Sox2 binding site (Table S1). The Lin28B plasmid in pBluescript II SK(+) was ordered from Gene Universal. Large scale PCR reactions (10-60 ml) were prepared as described[59] using unlabeled DNA primers or 5′-end labeled fluorescent primers (6-FAM, Cy3) obtained from IDT with HPLC purification. PCR product was purified by vertical gel electrophoresis on a 6% (60:1 Acrylamide/Bisacrylamide) native gel column using a 491 Prep Cell (Bio-Rad) run at 11 W and 4 °C, as described.[64] Fractions were analyzed via agarose gel, concentrated, and stored at -20 °C.

Nucleosome preparation

Lyophilized histones were resuspended in 20 mM Tris-HCl pH 7.8, 6 M Guanidine-HCl, 5 mM DTT at roughly 2 mg/mL with approximately 15-20% molar excess of H2A/H2B and refolded by dialyzing 4 times into Refolding Buffer (10 mM Tris-HCl pH 7.8, 2 M NaCl, 1 mM EDTA, 5 mM BME) using a 3.5kDa membrane (Spectra Labs) at 4°C. The refolded octamer (and excess H2A-H2B dimer) was then concentrated and purified by using a HiLoad 16/600 Superdex 200 pg column (Cytiva), as described.[63, 64] Fractions were analyzed by SDS-page gel, concentrated to 50-150 μM, flash frozen, and stored at -80°C. Nucleosomes were reconstituted following an adapted salt-dialysis protocol,[63, 64] where purified octamer (6 μM), dimer (1.8 μM), and 10% excess of DNA (6.6 μM) were combined. Nucleosomes were concentrated and purified via vertical gel electrophoresis as for DNA, except using a 7% (60:1 Acrylamide/Bisacrylamide) native gel column.[59]

EMSA

10 nM of 5′-FAM/5′-Cy3-labeled nucleosome (NCP) was mixed with variable concentrations of Sox2 HMG or Oct4 (CtoS mutant) protein (10 nM to 300 nM) in binding buffer (10 mM Tris-HCl pH 7.5, 150 mM KCl, 1 mM EDTA pH 8.0, 1 mM DTT, 0.5 mg/ml Recombinant Albumin (NEB), 5% glycerol) in a total reaction volume of 20 μL and incubated at 25 °C for 45 min. Reactions were loaded (2 μL) on a 5% native polyacrylamide gel and run for 120 min at 100 V on ice. Binding was visualized using a Typhoon 5 imager (GE Amersham) using FAM fluorescence.

DnaseI Footprinting

Reactions were set up in 10 mM Tris-HCl pH 7.5, 100 mM KCl, 1 mM DTT, 0.2 mg/ml Recombinant Albumin (NEB), 0.02% Tween-20, 8% Glycerol, containing 100 nM Lin28B DNA or NCP. Binding reactions were set up with or without Sox2 HMG (0.1 μM or 1 μM), and Oct4 CtoS (0.5 μM or 5 μM), and incubated at 25 °C for 45 min. DNaseI (NEB) was added at 0.5 U (or 0.125 U) for NCP and 0.1 U (or 0.025 U) and incubated for 5 min at 25°C, inactivated by 40 μL quench buffer and heat, as previously described.[59] DNA was purified using Phenol-Chloroform extraction and ethanol precipitated. Samples were run on a denaturing sequencing gel.[59] Gels were scanned on a Typhoon 5 imager (GE Amersham) as described for EMSA. Gel lane analysis was performed with ImageJ2[65] using background subtraction and contrast adjustment. Minor groove analysis was performed using the X3DNA server.[52] The change in minor groove width for bound versus unbound was obtained using the following structures: PDB ID: 6T7B (unbound) and 6T79 (Sox2-bound) for SHL+2;[57] PDB ID: 6T93 (unbound) and 6T90 (Sox2-Oct4-bound) for SHL-6; PDB ID: 6YOV (unbound) and 6T90 (Sox2-Oct4-bound) for SHL+6.[58]

Exonuclease III assay

Reactions were set up in 10 μL of 10 mM Tris-HCl pH 7.5, 150 mM KCl, 1 mM DTT, 1 mM EDTA, 0.2 mg/ml BSA, 0.02% Tween-20, 8% Glycerol containing 100 nM NCP, with or without Sox2 HMG (0.3 to 1 μM), and/or Oct4 (1 to 3 μM), and incubated at 25 °C for 45 min. ExonucleaseIII (NEB) dilutions were created with equal parts stock enzyme (100 U/μL) and reaction buffer supplemented with 76.67 μM $MgCl_2$). 1.5 μL of enzyme dilution or reaction buffer was added and incubated for desired time. Reaction was stopped with 40 μL quench buffer (10 mM Tris pH 7.5, 20 mM EDTA, 1.2% SDS, 100 ng/μl glycogen) and inactivated at 75 °C for 20 min. DNA was purified using Phenol-Chloroform extraction and ethanol precipitated. Samples were prepared and run on a denaturing sequencing gel, quantified, and analyzed as described for DNaseI footprinting.

Restriction Enzyme Digest

Reactions were set up in 20 μL rCutsmart buffer (NEB) using 10 nM NCP on ice and 10 U of MslI (NEB). Then reactions were incubated for 2 hrs at 25 °C or 37 °C, quenched with 60 μL Quench buffer (50 mM Tris Acetate pH 7.5, 50 mM EDTA pH 8, 2% SDS, 0.2 mg Glycogen), and heated at 85ºC for 20 min. Samples were prepared using Phenol-Chloroform extraction, ethanol precipitated, and resuspended in 10 μL Orange G Formamide dye as described in DnaseI assay. 5 μL of reaction was loaded onto an 8 M Urea/8% Acrylamide gel and run for 2 hrs at 130 V. Gels were imaged as described in EMSA.

FRET

Reactions were set up in 120 μL EMSA binding buffer containing 20 nM NCP or DNA with 5′-(6-FAM)/5′-Cy3 labeling. For binding, proteins (Sox2 HMG, Oct4 CtoS) were diluted into buffer and added at a 200 nM final concentration. Fluorescence emission scans were measured on an ATF 105 Differential/Ratio Spectrofluorometer (AVIV). For FRET, FAM was excited at 495 nm and data was collected for 505-600 nm range. To subtract background signal, that ratio of intensity at 560 nm (I_{560}) to intensity at 520 nm (I_{520}) for 5 different 145 base pair 601* DNAs or Lin28B DNA was calculated (0.412 ± 0.015) and applied to the NCP spectra. The corrected acceptor intensity ($I_{A,corr}$) and FRET ratio were calculated as follows: $I_{A,corr} = I_{560} - I_{520}(0.412 \pm 0.015)$; $FRET_{corr} = I_{A,corr} /(I_{520} + I_{A,corr})$. FRET values represent the average and standard deviation of 2 or more technical replicates and 2 or more experimental measurements. The spectra for FAM-only labeled NCP and DNA were identical. A Cy3-only labeled DNA, excited using FAM parameters, showed no contribution to I_{520}.

NMR spectroscopy

Nucleosome samples were prepared with a single isotopically labeled histone (^{15}N- or ^{15}N,^{13}C-labeled H3, H2A/H2A.Z or H4). Samples were dialyzed 3 times against NMR buffer (20 mM Tris-HCl pH 7.0, 25 mM NaCl, 0.5 mM TCEP, 1 mM EDTA) using a 3.5 kDa membrane (Spectra Labs) and further concentrated to ~20 μM (~300 μl) using an Amicon Ultra-0.5 (10 kDa) centrifugal device at 4°C. For Sox2 titrations, 50 μM unlabeled Sox2 HMG was added slowly to NCPs at appropriate ratios and concentrated to ~300 μL as above. The (^{15}N-H2A)-H2B dimer sample was prepared at 20 μM by exchanging into NMR buffer, as for NCPs. To make the histone dimer-DNA complex, dimer was slowly added to a 2-fold excess of a DNA40 duplex containing the mFgf4 motif (see Table S1). The NMR buffer was supplemented with 7.5% D_2O (CIL) prior to experiments. Data was collected on a Bruker Ascend 800 MHz NMR spectrometer equipped with a triple-resonance cryoprobe using standard 2D ^{1}H-^{15}N HSQC experiments (64 scans) at 25 °C and 37 °C. Data was processed using nmrPipe[66] and analyzed using Sparky[66] and in-house scripts. H3 N-tail peak intensities were normalized to a resolved residue (K14) with small fluctuations across samples. Chemical shift perturbations (CSPs) were calculated from the difference in proton ($\Delta\delta_H$) and nitrogen ($\Delta\delta_N$) chemical shifts in ^{1}H-^{15}N HSQC spectra, as follows: $CSP = (\Delta\delta_H^2 + (0.154\Delta\delta_N)^2)^{1/2}$.

Molecular Dynamics Simulation

The DNA sequence and initial configuration of the nucleosome core particle (NCP) were obtained from the crystal structure PDB ID: 3LZ0[67] missing the histone N-terminal tails and the C-terminal tail of H2A. The N-terminal tails and other missing residues were modeled following our previous work.[31] The canonical nucleosome containing H2A was modeled with the addition of the C-terminal tail (KTESSKSKSK), using Chimera.[68] The dihedral angles for each residue in the C-terminal histone H2A tails were assigned with φ angle = -60° and ψ angle = 30°. The H2A.Z nucleosome was modeled using PDB ID: 1F66[69] by swapping canonical H2A from the above construct with H2A.Z. The final NCP constructs for both H2A and H2A.Z were visualized using PyMOL and VMD.[70] Both H2A and H2A.Z nucleosome constructs were parameterized using AMBER forcefields at 150 mM NaCl concentration under physiological conditions. The histone was simulated with ff19SB,[71] and DNA was parameterized using OL15.[72] The OPC water model[73] was used, with its Lennard-Jones interaction (Na^+/OW) modification, using the Kulkarni *et al*. method, which provides better estimates of osmotic pressure.[74] For sodium (Na^+) and chlorine (Cl^-) ions, Joung and Cheetham[75] parameters were used. Mg^{+2} modification was performed using the Li *et al* parameter method.[76] All systems were initially minimized and heated using Amber22.[77] The systems were equilibrated for 100 ns, followed by production runs for 1 μs using GROMACS 2022.5.[78] See SI Methods for more information on MD setup and data analysis.

Results

H2A.Z stimulates DNA unwrapping in a sequence-dependent manner

Prior studies have reported potential interaction and functional coordination between histone variant H2A.Z and pioneer factors Sox2 and Oct4.[7, 21, 25, 26] To probe the effect of H2A.Z on the interaction of Sox2 and Oct4 with chromatin, we constructed nucleosome core particles (NCPs) with (i) a modified 145 base pair Widom 601 sequence (601*) with Sox2-Oct4 composite motifs inserted at different positions or (ii) a 147 base pair fragment from the human Lin28B enhancer that naturally contains several putative Sox2 and Oct4 binding sites (Table S1).[56] For composite motifs in 601* NCPs, we used sequences derived from mouse Nanog (mNanog, N)[51] and Fgf4 (mFgf4, F)[79] gene regulatory elements, and inserted them at previously characterized positions.[59]

We first asked whether H2A.Z would increase the mobility and unwrapping of nucleosomal DNA, as observed before.[44, 47] To assess changes in DNA accessibility due to unwrapping, we used nuclease digestion and bulk Förster resonance energy transfer (FRET) assays (Figure 1). The extent of digestion by Exonuclease III (ExoIII), which degrades DNA progressively from the 3' end of each strand, was monitored as a function of time by denaturing gel electrophoresis with base-pair resolution (Figure 1A, Figure S1). Overall, for 601* and Lin28B NCPs, we observed faster and more extensive ExoIII digestion at both ends of the nucleosome with H2A.Z as compared to H2A. 601* constructs showed enhanced digestion with H2A.Z, primarily on the TA-rich side of the nucleosome (Figure 1A). Variable sensitivity to H2A.Z was also observed across DNA sequences differing by the position of the Sox2-Oct4 motif (Figure 1A, Figure S1). The effect of H2A.Z in Lin28B NCP extended deeper into the nucleosome core, consistent with greater destabilization (Figure 1A). Our results imply that H2A.Z facilitates unwrapping in a DNA sequence dependent manner, leading to asymmetric changes in nucleosome dynamics. As a control for enhanced unwrapping, we prepared corresponding nucleosome constructs with a histone H3 R49A mutation (Table S2) eliminating a key interaction with the minor groove of DNA at entry/exit points of the nucleosome. As expected, digestion in control H3 R49A NCPs was even more pronounced (Figure 1A, Figure S1), consistent with increased unwrapping upon disruption of histone-DNA contacts. These results were confirmed in a separate endonuclease assay, where the restriction enzyme MslI was used to cleave DNA sequence-specifically at the Sox2-Oct4 motif near SHL+6 or -6 (Figure S1).

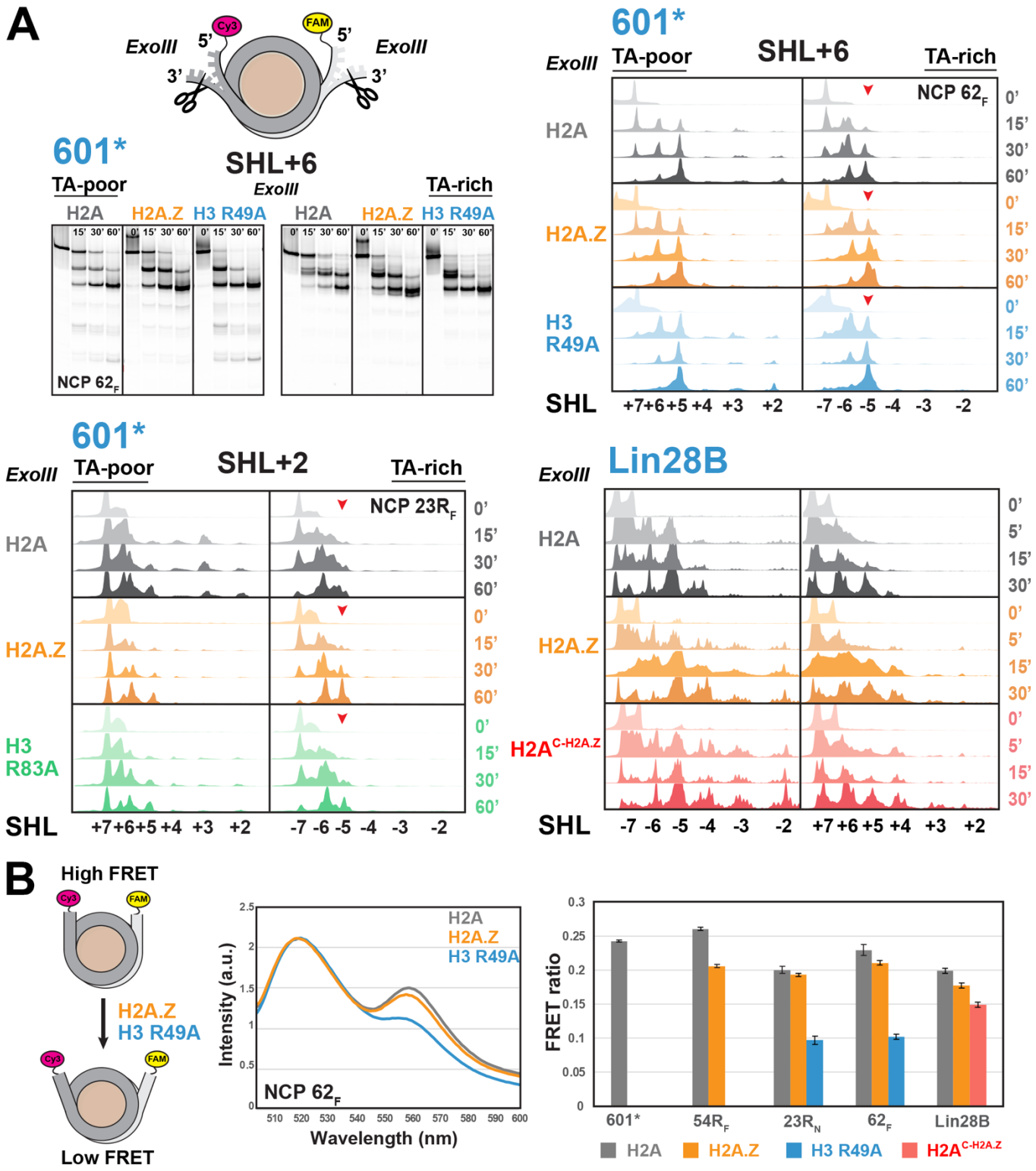

Figure 1. H2A.Z stimulates DNA unwrapping in 601* and Lin28B nucleosomes. (A) Exonuclease III (ExoIII) digestion time course of (i) 601* NCPs with a Sox2-Oct4 motif at SHL+6 (NCP 62_F) or SHL+2 (NCP $23R_F$), and (ii) Lin28B NCPs containing H2A, H2A.Z, or histone mutants. Faster ExoIII digestion, indicating increased DNA accessibility, is observed with H2A.Z, $H2A^{C\text{-}H2AZ}$, and H3 R49A relative to H2A. Data was plotted from analysis of denaturing gels, monitored by Cy3 (left) and FAM (right) fluorescence. (B) FRET assay of nucleosome constructs labeled with FAM and Cy3 probes (left) used to detect unwrapping. Sample fluorescence spectra of NCP 62_F obtained by FAM excitation at 495 nm (center), showing a decrease in Cy3 fluorescence at 560 nm (lower FRET) with H2A.Z and H3 R49A. FRET ratios (right) for NCP constructs depicting increased unwrapping for most H2A.Z and, especially, H3 R49A constructs, and a large DNA sequence dependence.

We noted increased ExoIII digestion penetrating internal sites up to SHL+2 on the TA poor side of canonical 601* nucleosomes, which varied with the position of the Sox2-Oct4 motif (Figure 1A, Figure S1). Surprisingly, the internal cleavage was typically suppressed with H2A.Z, but not with the destabilizing H3 R49A mutant, and persisted only when the Sox2-Oct4 motifs were placed at SHL+5 (Figure 1A, Figure S1). To test whether increased internal DNA mobility plays a role, we used an H3 R83A mutant that disrupts an arginine-DNA minor groove interaction at SHL+/-2. As expected, the mutant displayed a local enhancement in ExoIII digestion at SHL+2 (Figure 1A, Figure S1). Thus, it seems that H2A.Z can simultaneously destabilize DNA ends and stabilize nucleosomes internally in a DNA sequence dependent manner. Our observations are in line with a previous study showing that H2A.Z can both destabilize peripheral DNA and inhibit H2A-H2B dimer dissociation from the H3-H4 tetramer upon thermal denaturation of nucleosomes.[80]

To monitor directly H2A.Z-induced DNA unwrapping, we measured FRET between the fluorophores FAM and Cy3 covalently attached to the 5' ends of DNA (Figure 1B). We expected that enhanced unwrapping would increase the average distance between the two probes and therefore decrease the FRET efficiency. Here, the FRET efficiency (expressed as FRET ratio) was visibly reduced with H2A.Z as compared to H2A in nearly all NCP constructs (Figure 1B). The only exception was NCP $m62_F$, which also showed lower sensitivity to H2A.Z in ExoIII assays (Figure S1). Relative FRET changes were also dependent on the position and identity of the Sox2-Oct4 motif (Figure 1B, Figure S2). Specifically, the effects were smaller for SHL+2 and SHL+6 but larger for SHL+5 (Figure S2). This variation could signify that H2A.Z nucleosomes are more sensitive to DNA sequences with a stretch of AT base-pairs (i.e. A-tracts) at SHL+5 contained within the mFgf4 motif, and is supported by the increased internal ExoIII digestion with H2A.Z in NCP $54R_F$ (Figure S1). Together, our results show that entry/exit DNA unwrapping is enhanced by H2A.Z and modulated by variations in DNA sequence.

H2A.Z enhances Sox2 and Oct4 binding to 601 nucleosomes

We next asked if the observed H2A.Z-induced changes in nucleosome stability and dynamics would alter the binding of Sox2 and Oct4. To assess this, we used a native gel shift assay (EMSA) under near physiological salt conditions (150 mM KCl) (Figure 2, Figure S3). When the Sox2-Oct4 motifs were placed close to the nucleosome edge, at SHL-6 (NCP $m62_F$ and $m62_N$) and SHL+6 (NCP 62_F and 62_N) of 601*, the stability of the Sox2-nucleosome complex was visibly increased with H2A.Z (Figure 2B). This was evident for both mFgf4 (F) and mNanog (N) composite motifs. Sox2 association with H2A.Z nucleosomes was additionally enhanced when the Sox2-Oct4 motif was inserted at the internal site at SHL+2 (NCP $23R_F$ and $23R_N$). By contrast, Sox2 binding was not significantly altered by H2A.Z at a high-affinity binding site near SHL+5 (NCP $54R_F$ and $54R_N$) (Figure S3).[59] This data suggests that H2A.Z can enhance Sox2-nucleosome binding in a position dependent manner, for both internal and terminal sites.

H2A.Z affected the binding of Oct4 to end-positioned sites on 601* nucleosomes in an asymmetric manner (Figure 2C, Figure S3). For NCP 62_N (SHL+6, TA poor side), where the Oct4 mNanog POU_S half-site is exposed and the POU_{HD} half-site occluded, H2A.Z facilitated formation of the specific Oct4-NCP complex (Figure 2C). By contrast, when the Oct4 mNanog motif was placed at SHL-6 (NCP $m62_N$) on the TA-rich side, which we observed to be more unwrapped by ExoIII digestion (Figure S1), the specific complex formed equally well on canonical and H2A.Z NCPs (Figure 2C). This was also noted with the destabilizing H3 R49A mutant (Figure 2C). By contrast, with nucleosomes that contain the mFgf4 motif at SHL+6/-6 (NCP 62_F and $m62_F$) where only the POU_{HD} half-site is solvent accessible, only H2A.Z enhanced formation of the specific complex (Figure S3). This strong effect of H2A.Z but lack of sensitivity to DNA unwrapping (H3 R49A) could mean that either Oct4 binds at a different than

expected site or that H2A.Z employs a different mechanism. Overall, our results point to a role of H2A.Z-induced DNA unwrapping in Oct4-nucleosome association.

Using FRET, we further observed deformation of entry/exit DNA induced by Sox2 binding (Figure S2). This effect was enhanced by the synergistic binding of Sox2 and Oct4 and even more marked in the presence of H2A.Z (Figure S2). These results validate our previous findings that the folded conformation of Sox2, and large DNA bending, is stabilized by Oct4 on adjacent motifs at SHL6.[59]

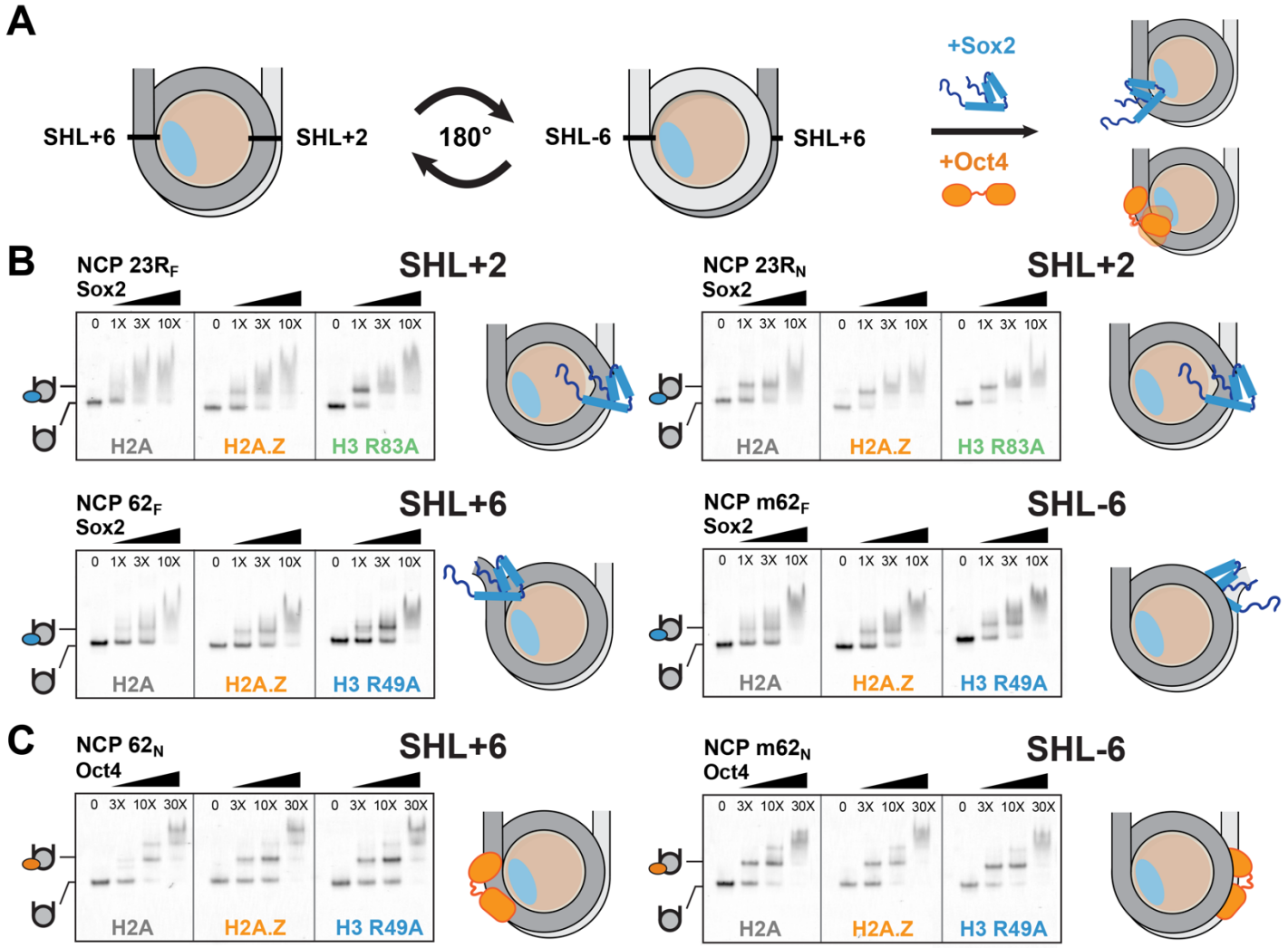

Figure 2. H2A.Z promotes Sox2 and Oct4 binding at end-positioned and internal motifs on 601* nucleosomes. (A) Approximate position of Sox2-Oct4 composite motifs (black lines) near SHL+2, +6, and -6 shown in relation to H2A/H2A.Z (light blue). (B) EMSA gels of NCPs (10 nM) in the presence of increasing concentrations of Sox2 (10, 30, and 100 nM) showing improved Sox2 binding with H2A.Z at SHL+2 and SHL+6/-6. Additionally enhanced binding is observed with H3 R83A and H3 R49A mutant NCPs, used as controls for locally increased DNA mobility at SHL+2 and SHL+/-6, respectively. Gels were visualized by FAM fluorescence. (C) EMSA gels of NCPs (10 nM) in the presence of increasing concentrations of Oct4 (30, 100, and 300 nM) showing formation of a more stable specific Oct4-NCP complex with H2A.Z and H3 R49A at SHL+6 (TA-poor side), but not at SHL-6 (TA-rich side), where the DNA is already more unwrapped (see Figure 1A).

The Lin28B nucleosome is significantly less stable than 601, as seen by ExoIII digestion (Figure 1A), and is known to exhibit greater dynamics[81] and heterogenous positioning *in vitro*.[45] Surprisingly, we did not detect a large H2A.Z effect on Sox2 binding to Lin28B NCP (Figure 3B). Using EMSA, we observed one major super-shifted band at an equimolar ratio of canonical NCP and Sox2 and multi-site binding at higher protein concentrations. With H2A.Z, we observed an additional “ladder” effect at low Sox2

ratios (Figure 3B) that could be attributed to H2A.Z or, alternatively, to binding of Sox2 to a small amount of naked DNA (data not shown). Oct4 showed ubiquitous binding to the canonical Lin28B NCP and small enhancement with H2A.Z (Figure 3B), as well as a similar ladder effect. The lesser effect of H2A.Z could be due to the suboptimal orientation and/or more internal positioning of Sox2 and Oct4 motifs on Lin28B nucleosomes (Figure 3B).

Sox2 induces an altered conformation in Lin28B nucleosomes, enhanced by H2A.Z

To further investigate where Sox2 binds on Lin28B nucleosomes, we used limited DNaseI digestion (Figure 3, Figure S4). Lin28B contains four minimal Sox2 recognition motifs (TTGT) (Figure 3A) and can interact extensively with Sox2.[56] Here, for both NCPs, we detected multiple regions of reduced DNaseI cleavage (footprints) alternating with regions of increased cleavage (hypersensitive sites) (Figure 3C). Similar patterns were observed at two DNaseI concentrations and likely not produced by over-digestion (Figure S4). Importantly, Sox2-induced hypersensitive sites were absent with naked DNA, 601* NCP, and no DNaseI controls (Figure S4). Footprints occurred almost periodically at positions, where the DNA minor groove faces outward and away from the histone core, and extended beyond TTGT motifs. At the same time, maxima of DNaseI cleavage were typically found at inward-facing minor groove positions (Figure 3C). While the H2A.Z NCP exhibited nearly the same pattern, enhanced cleavage was noted immediately next to the dyad, becoming more pronounced in the presence of Sox2 (Figure 3C). The higher DNaseI susceptibility at the dyad is consistent with the more extensive DNA unwrapping observed with H2A.Z (Figure 1).

It is tempting to explain the DNaseI footprints and hypersensitive sites as a direct result of multiple Sox2 binding events. Sox2 can locally bend nucleosomal DNA, compressing the minor groove nearby and exposing buried sites that can result in higher nuclease activity (Figure S4). While Sox2 produced many footprints on Lin28B DNA consistent with the multi-site binding in EMSA, there was no increased cleavage resulting from Sox2-induced deformations (Figure S4). With the Lin28B NCP, by contrast, hypersensitive sites mapped semi-regularly to buried minor groove positions (Figure 3C). Therefore, this profile likely reflects a change in DNA mobility or repositioning specific to nucleosomes. This is supported by the increased ExoIII digestion of Lin28B NCPs in the presence of Sox2 (Figure S4). One possibility is that Sox2 association shifts the DNA register in the context of less stable nucleosomes such as Lin28B. Unfortunately, our initial attempts to detect nucleosome sliding via histone-DNA crosslinking at SHL+/-5 were not successful, possibly due to large unwrapping and poor crosslinking efficiency (data not shown). Additional studies using more appropriate NCP constructs are ongoing.

The further addition of Oct4 enhanced the effect of Sox2 in DNaseI assays (Figure S4). This result is consistent with Oct4 stabilizing Sox2 binding and coupled changes in DNA conformation.[59] While Oct4 alone showed ubiquitous binding to Lin28B NCPs based on both EMSA and DNaseI digestion, it did not generate hypersensitive sites (Figure 3B, Figure S4). The cryo-EM structures of Lin28B NCP in complex with one or three Oct4 molecules also did not show significant DNA repositioning, except for asymmetric unwrapping.[61] Thus, the change in Lin28B nucleosome conformation is unique to Sox2 and not purely due to DNA unwrapping.

The H2A.Z C-terminal tail contributes to nucleosome dynamics

The C-terminal region (C-tail) of H2A.Z, which is shorter and less positively charged than that of H2A, has been implicated in increased dynamics at entry/exit points of nucleosomes.[44, 47] To test if the H2A.Z C-tail stimulates unwrapping and explains the enhancement in Sox2 binding, we engineered two C-tail swap mutants (Table S2, Figure S5). In the $H2A^{C\text{-}H2A.Z}$ construct, the last ten residues of H2A were replaced with the last six residues of H2A.Z, and vice versa for the $H2A.Z^{C\text{-}H2A}$ construct. We hypothesized that, if the H2A.Z C-tail was responsible for the increase in DNA unwrapping, then the

H2A$^{C\text{-}H2A.Z}$ mutant will mimic the dynamics and Sox2 binding behavior of H2A.Z, while the H2A.Z$^{C\text{-}H2A}$ mutant will restore the behavior of H2A.

Figure 3. Sox2 binding at multiple motifs alters the conformation of Lin28B nucleosomes, which is modulated by H2A.Z. (A) Lin28B sequence depicting potential binding motifs (TTGT) for Sox2 HMG (blue) and Oct4 POU$_S$ and POU$_{HD}$ domains (orange). NCP cartoons depicting approximate locations of Sox2 motifs (blue) and Sox2 DNaseI footprints (gray), and the position of H2A/H2A.Z (light blue). (B) EMSA gels of nucleosomes with increasing Sox2 (left) or Oct4 (right) concentrations, showing similar multi-site binding with both H2A and H2A.Z. The laddering effect with H2A.Z could be an artifact of more free DNA present in those samples. (C) DNaseI digestion profiles of H2A and H2A.Z Lin28B nucleosomes (100 nM) with or without Sox2 (1000 nM), showing multiple footprints (decreased signal) and hypersensitive sites (increased signal) in the presence of Sox2. The location of Sox2 footprints (grey, open) and TTGT motifs (blue) are indicated. The nucleosome dyad, showing higher DNaseI and Sox2 sensitivity with H2A.Z, is highlighted in red.

As hypothesized, installing an H2A.Z C-tail in the canonical histone (H2A$^{C\text{-}H2A.Z}$) led to larger DNA unwrapping in 601* and Lin28B NCPs based on enhanced ExoIII digestion and reduced FRET relative to H2A counterparts (Figure 1A, Figure S5). However, replacing the H2A.Z C-tail with that of H2A (H2A.Z$^{C\text{-}H2A}$) also had a sizeable destabilizing effect (Figure S5), implying that residues outside of this tail region contribute to dynamics. While we observed increased DNA dynamics in H2A$^{C\text{-}H2A.Z}$, the Sox2-NCP complex stability by EMSA did not visibly improve (Figure S5). This suggests that the H2A.Z C-tail alone is not responsible for the differential dynamics and Sox2 binding. To test this, we designed

two other H2A.Z mutants, one where either the N-terminal tail (H2A.Z-N^{H2A}) or L1 loop connecting α-helix 2 and 3 (H2A.Z-L1^{H2A}) is replaced with corresponding fragments from H2A (Table S2, Figure S5). We found that the marked internal digestion on the TA-poor side of most canonical NCPs, which was suppressed with H2A.Z, was restored with both the L1 loop and C-tail mutants (Figure S5, Figure S1). This suggests that perturbations in either the C-tail or L1 loop of H2A.Z can affect DNA dynamics. Also, the H2A.Z L1 loop, which has been proposed to alter dimer orientation and strengthen hydrogen bonding networks between histones and DNA,[46] may be partially responsible for this internal stabilization. Further targeted mutagenesis, combined with computation, could help establish the specific residues involved and allosteric networks that drive those perturbations.

H2A.Z alters the dynamics of the histone H3 N-terminal tail

In order to further explore the effect of H2A.Z on the conformation and dynamics of nucleosomes, we used solution NMR spectroscopy. We prepared H2A or H2A.Z containing nucleosomes with a single uniformly ^{15}N-labeled or ^{15}N,^{13}C-labeled histone (H3, H4, H2A or H2A.Z), where the Sox2-Oct4 composite motif was placed at SHL+6 (NCP 62$_{F/N}$), SHL+5 (NCP 54R$_F$), or SHL+2 (NCP 23R$_N$). For samples prepared at 20 μM in 7.5% D_2O NMR buffer, we could readily observe backbone amides of the flexible N- and C-terminal tails of each labeled histone using standard ^{1}H-^{15}N HSQC experiments.

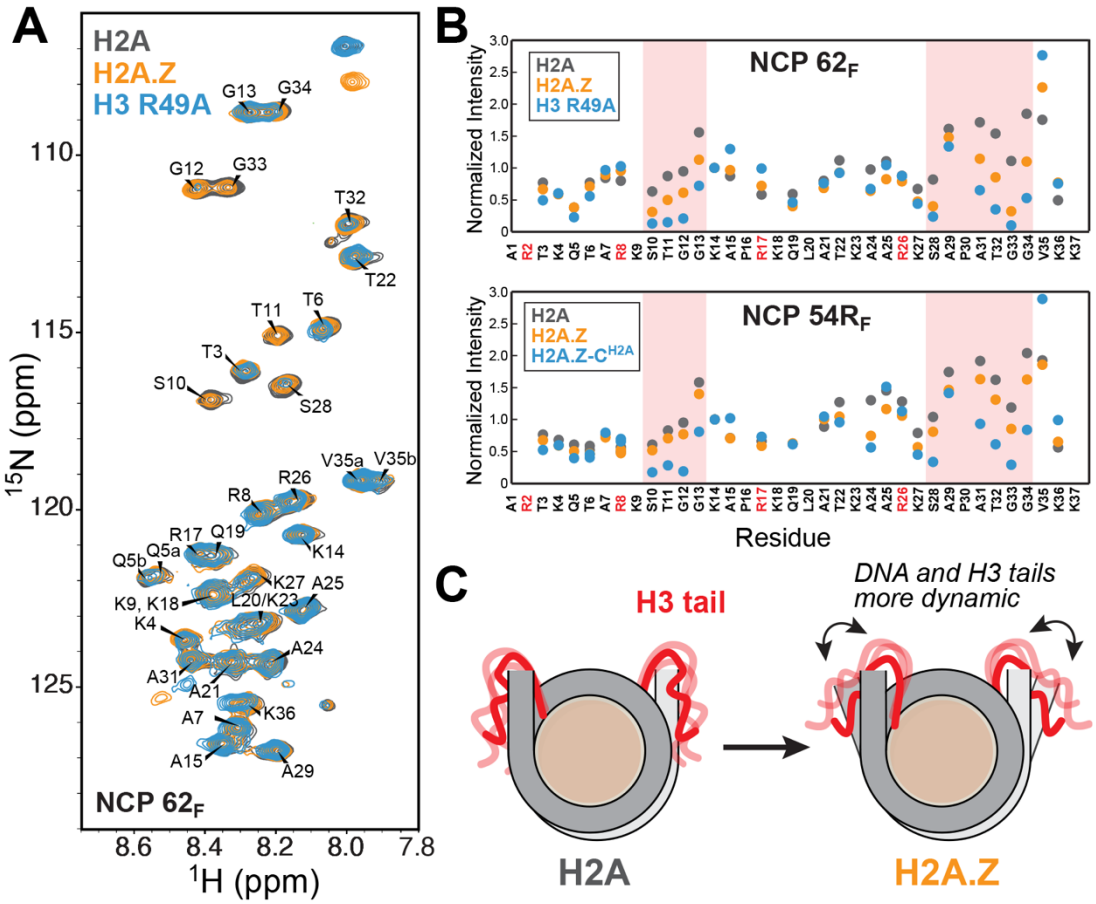

Figure 4. H2A.Z perturbs the dynamics of the H3 N-terminal tail in nucleosomes. (A) Overlay of ^{1}H-^{15}N HSQC spectra of ^{15}N-H3 NCP 62$_F$ (20 μM) containing H2A, H2A.Z or H3 R49A (37 °C) showing differences in resonance peak intensities and chemical shifts. (B) Normalized peak intensities obtained from spectra in (A) (top) showing decreased values for residues in flexible "hinge" regions (S10-G13 and S28-G34) with H2A.Z and, especially, with H3 R49A. Similar results are obtained for NCP 54R$_F$ (bottom) with H2A.Z and the H2A.Z$^{C\text{-}H2A}$ mutant observed to be destabilized in ExoIII assays (Figure S6). (C) Cartoon of H3 N-tails showing perturbed dynamics with H2A.Z.

We first compared the backbone amide HSQC spectra of the H3 N-terminal tails of H2A and H2A.Z NCPs. Using published assignments,[82] we quantified changes in peak intensities (Figure 4A) and chemical shifts to obtain information on changes in backbone structure and dynamics. While chemical shifts remained unaffected, we observed large changes in the relative intensities for two H3 N-tail regions – residues 10-13 and 27-34. These regions act as flexible "hinges" due to their greater mobility, previously characterized by NMR.[83] Specifically, for NCP 62_F and $54R_F$ containing the mFgf4 motif, peak intensities of hinge residues were diminished in H2A.Z as compared to H2A NCPs (Figure 4B). This is consistent with an increase in chemical exchange dynamics on the micro-to-millisecond (*μs-ms*) timescale. Intensities for the same residue were further attenuated with less stable constructs, $H2A.Z^{C\text{-}H2A}$ (NCP $54R_F$) and, especially, with H3 R49A (NCP 62_F) (Figure 4B). This data suggests a correlation between differential H3 N-tail dynamics and increased DNA unwrapping associated with these mutants.

For nucleosomes containing the mNanog motif (NCP 62_N and $23R_N$), the same hinge regions showed instead an increase in peak intensities with H2A.Z, further enhanced by the destabilizing $H2A.Z^{C\text{-}H2A}$ (NCP 62_N) and H3 R83A (NCP $23R_N$) mutants (Figure S6). One way to interpret this is as increased fluctuations on the picosecond-to-nanosecond (*ps-ns*) timescale, occurring faster than the predicted rotational correlation time of ~114 ns for a free nucleosome.[84] It is quite possible that the inverse effect on intensities in mNanog versus mFgf4 NCPs results from different contributions of slow *(μs-ms*) and fast (*ps-ns*) dynamics. We note that, based on FRET efficiencies (Figure 1B, Figure S2) mNanog NCPs are on average more unwrapped than mFgf4 ones, which likely correlates with altered H3 N-tail dynamics. Unfortunately, the low sample concentrations prevented us from accurately quantifying NMR relaxation rates that can be used to extract motional parameters. Further experiments would be needed to elucidate the dynamics at different timescales and their dependence on DNA sequence and variant.

Sox2 competes with the H3 N-terminal tail for DNA binding at multiple nucleosome sites

Our data implies that the H3 N-tail in H2A.Z nucleosomes has reduced contacts with DNA, which can facilitate Sox2 binding. To probe how association of Sox2 affects the conformation and dynamics of the H3 N-tail, we performed titrations of canonical and H2A.Z NCPs with Sox2 and observed the H3 amide chemical shifts (Figure 5, Figure S7). The largest chemical shift perturbations (CSPs) occurred when Sox2 bound at SHL+6 (NCP $62_{F/N}$), in the vicinity of the H3 N-tail. Specifically, we observed the emergence of a second set of peaks shifted in the direction of the free H3 N-tail peptide (Figure 5, Figure S7), previously assigned.[35] This is consistent with Sox2 competitively displacing one of the H3 N-tails from DNA. Residues around and including H3 arginine 26 (R26), 17 (R17), and 8 (R8), which serve as "anchor" points by maintaining stronger interactions with the DNA minor groove, exhibited the largest CSPs. Similar chemical shift trends were detected for H2A.Z and H3 R49A nucleosomes, with larger CSPs on average and especially for residues surrounding H3 R26 (Figure 5, Figure S7).

Surprisingly, we also observed smaller but distinct chemical shift changes in the H3 N-tail when the Sox2 motif was placed at more internal positions in 601* NCPs, SHL+5 (NCP $54R_F$) or SHL+2 (NCP $23R_N$), or with Lin28B NCPs (Figure 5, Figure S7). For these constructs, only a few peaks split into two distinct populations, consistent with more limited changes in conformation. Notably, the canonical Lin28B chemical shifts resembled more the free peptide, even without Sox2, indicating partial H3 N-tail dissociation. Overall, a greater effect was detected with H2A.Z and destabilizing mutants. For NCP $23R_N$, large CSPs were clustered around the first several residues (Figure 5, Figure S7), implying that Sox2 primarily peels off the tip of the N-tail. SHL+5 is near the N-tail interaction site, as seen by MD simulations,[34] while SHL+2 is found in closer proximity to the edge of the parallel DNA gyre. Thus, it is conceivable that Sox2 binding at these sites directly or allosterically disrupts interactions between DNA and the tip of the H3 N-tail. Our NMR data suggests that Sox2 competes with the H3 tail for DNA binding

at various nucleosome positions, which could have important consequences for Sox2 interaction with destabilized nucleosomes and, therefore, chromatin structure and histone tail recognition.

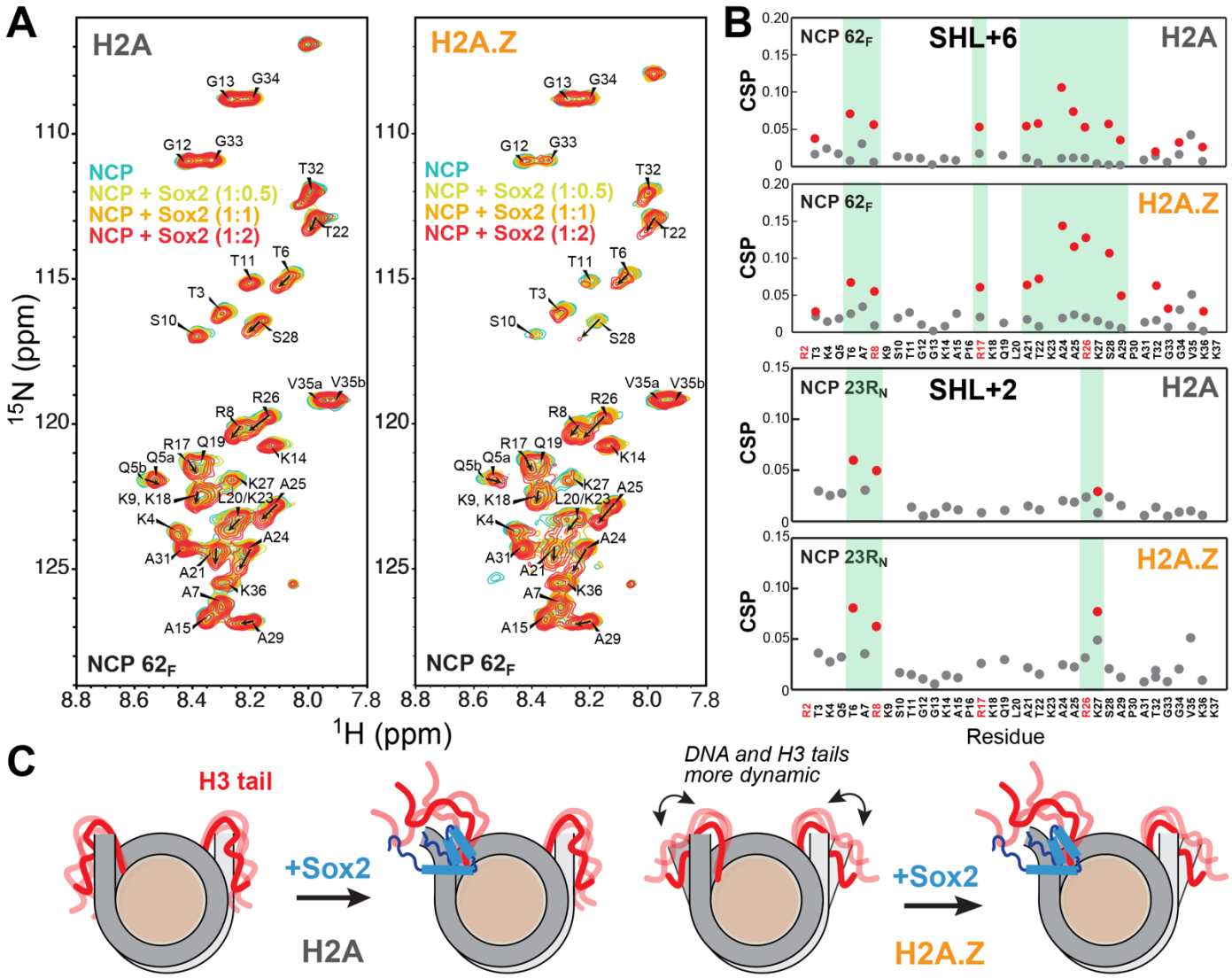

Figure 5. Sox2 displaces the H3 N-terminal tail from DNA, facilitated by H2A.Z. (A) ^{1}H-^{15}N HSQC spectral overlay of NCP 62_F (20 μM) containing ^{15}N-H3 and H2A (left) or H2A.Z (right) with increasing concentrations of Sox2 (10, 20, and 40 μM) obtained at 37 °C. Visible peaks represent the H3 N-terminal tail (residue 2-36). A second population of peaks is observed with Sox2 with chemical shifts closer to the free H3 N-tail peptide,[35] consistent with tail dissociation from DNA. (B) Chemical shift perturbations (CSP) for the H3 N-tail derived from Sox2 titrations of NCP 62_F with H2A or H2A.Z. The second population is shown with red circles. Large CSP values for residues around R8 and R26, which tend to become more pronounced with H2A.Z, are highlighted in green. (C) Cartoon showing H3 N-tail displacement upon Sox2 binding, facilitated by enhanced tail dynamics with H2A.Z.

Sox2 perturbs the C-terminal tail of H2A more than that of H2A.Z

We then asked if Sox2-nucleosome association at SHL6 and SHL2 could likewise be affected by competition with other histone tails, including the H2A C-tail and H4 N-tail. To probe this, we performed titrations of canonical and H2A.Z nucleosomes containing ^{15}N-labeled H2A/H2A.Z or H4 with Sox2 (Figure 6, Figure S8, Figure S9). Resonance assignments for H2A and H4 were transferred from published studies.[82, 85] For H2A.Z, we could unambiguously identify several residues and localize others based on characteristic chemical shifts and comparison between H2A, H2A.Z, and the C-tail swap mutant H2A.Z$^{C\text{-}H2A}$ NCP spectra (Figure 6, Figure S8).

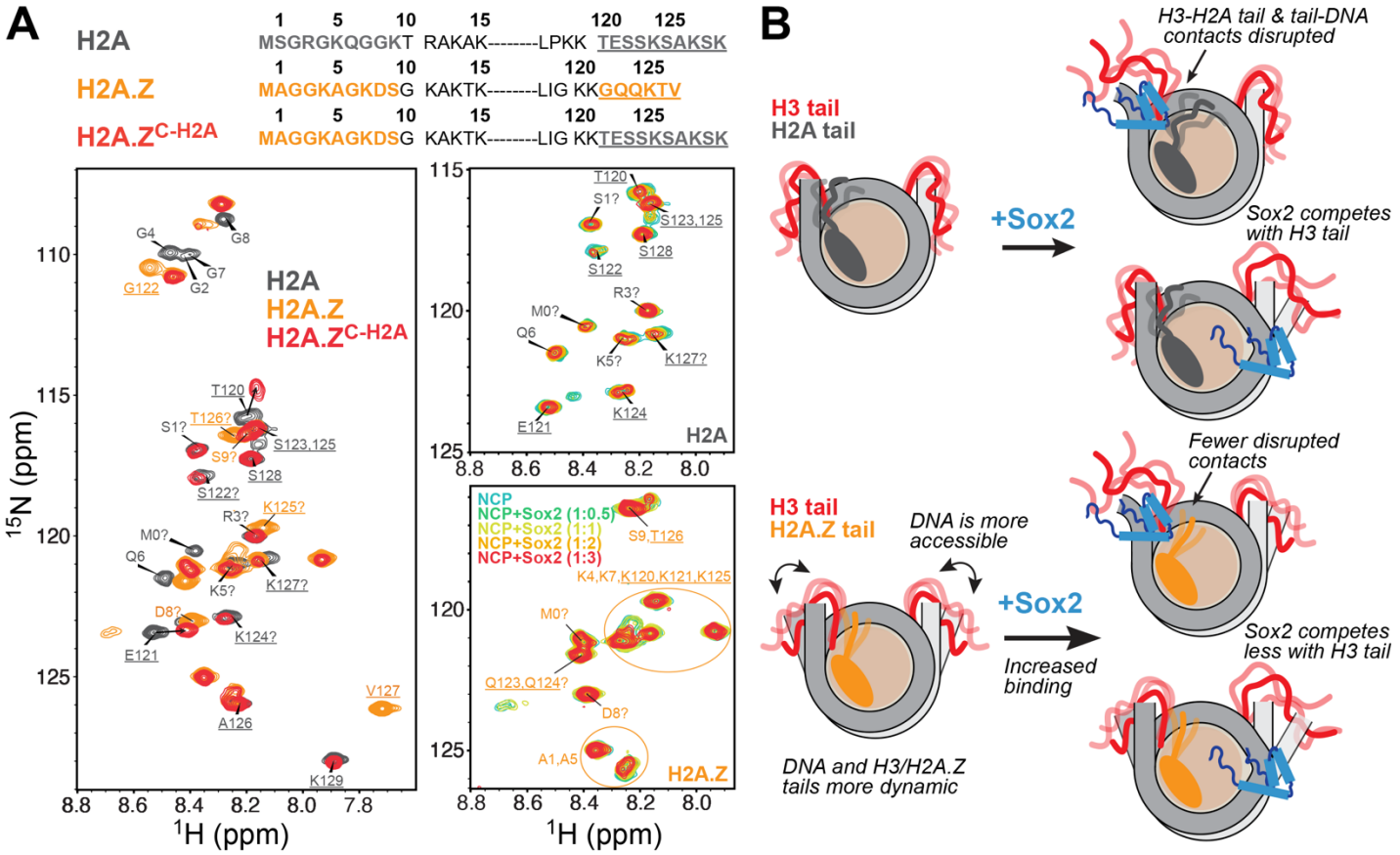

Figure 6. Sox2 perturbs the H2A C-terminal tail more than that of H2A.Z. (A) ^{1}H-^{15}N HSQC spectral overlay of free NCP 62_F (20 μM) containing ^{15}N-labeled H2A (grey), H2A.Z (orange), or H2A.Z$^{C\text{-}H2A}$ (red) on the left and corresponding NCP constructs with increasing concentrations of Sox2 (10, 20, 40 and 60 μM) on the right, obtained at 37ºC. The H2A C-tail shows larger chemical shift perturbations than that of H2A.Z and H2A.Z$^{C\text{-}H2A}$ (see Figure S8 for full spectra). Amino acid sequences (top) showing the visible residues of the N- and C-terminal tail regions for the same constructs in bold, with the C-tail underlined. (B) Proposed model for nucleosome destabilization and enhancement of Sox2 binding by H2A.Z. H2A.Z incorporation leads to weaker contacts between H3 tail, H2A.Z tail, and DNA and increased DNA accessibility, facilitating Sox2-nucleosome binding.

Addition of Sox2 caused marked chemical shift changes and line broadening in multiple residues in the H2A C-tail (and N-tail) in canonical NCPs (Figure 6A). By contrast, the effect of Sox2 on the H2A.Z C-tail was minimal. This suggests that, when Sox2 binds at SHL+6 (NCP 62_F), the H2A C-tail experiences larger conformational changes than the shorter H2A.Z C-tail. Moreover, the destabilized H2A.Z$^{C\text{-}H2A}$ mutant C-tail displayed significant differences in chemical shifts as compared to the H2A C-tail (Figure 6A). Glutamate 121 (E121) was strongly perturbed and, notably, its chemical shift closely matched that of E121 in the context of an H2A-H2B dimer bound to DNA (Figure S8). These changes are consistent with an altered E121 conformation or protonation state. Addition of Sox2 to H2A.Z$^{C\text{-}H2A}$ NCP also resulted in smaller CSPs for the same residues affected in H2A NCP (Figure S8). This data indicates the H2A.Z$^{C\text{-}H2A}$ C-tail adopts a different conformation than the H2A C-tail, which is closer to an H3-free state and is less perturbed by Sox2. Considering the larger DNA unwrapping observed in H2A.Z$^{C\text{-}H2A}$ (Figure S1), the smaller impact of Sox2 is likely due to weakened C-tail interactions with DNA and H3.

Finally, we monitored perturbations to the H4 N-tail as a result of Sox2 binding at SHL+2 (NCP $23R_N$) (Figure S9). The H4 N-tail adopted similar conformations in H2A and H2A.Z NCPs, as judged by their nearly identical spectra, and addition of Sox2 produced a negligible effect for both systems (Figure S9). Therefore, it is unlikely that the enhanced Sox2 binding at SHL+2 with H2A.Z can be explained by

changes in the conformation and dynamics of the H4 N-tail. Rather, a destabilized H3 N-tail coupled to higher DNA mobility could create more favorable energetics for Sox2 binding to H2A.Z nucleosomes.

Simulations show higher disorder and fewer DNA contacts of the H3 tail in H2A.Z nucleosomes

To further compare the conformational dynamics of DNA and histone tails for H2A and H2A.Z 601 nucleosomes, we performed 1 μs long MD simulations at physiological salt conditions (Figure 7A). The H2A.Z NCP showed increased DNA unwrapping from the SHL7 region, while DNA in the canonical NCP remained mostly bound to the histone octamer (Figure 7B). Based on our NMR data, we wondered how H2A.Z impacted the structure and dynamics of the H3 N-tail. In the H2A.Z system, we found that H3 N-tail conformations are less ordered and less helical (Figure 7C, Figure S10). This is coupled to repositioning of the H3 N-tail away from SHL2 and increasing the gaping distance for the two parallel DNA gyres (Figure S11). In the H2A system, the H3 N-tail was found to be more ordered and helical, and to adopt more extended conformations that maintain contacts with both DNA gyres, including SHL2 (Figure 7C, Figure S12). The bridging of DNA gyres by the H3 N-tail could have a stabilizing effect and suppress DNA unwrapping in canonical NCPs. Overall, the increase in DNA accessibility at SHL2 due to altered conformation and greater dynamics of the H3 N-tail in the H2A.Z system is consistent with the increase in Sox2 binding there (Figure 2). To further analyze the H3 dynamics, we calculated structural fluctuations as root-mean-square fluctuations (RMSF) (Figure 7D). Overall, H3 in the H2A.Z system showed higher fluctuations relative to the H2A system, especially, for residues 7-9, 12-16, and 21-33 of the H3 N-tail. This supports our NMR data that displays large changes in the relative intensities for a similar set of residues (Figure 4, Figure S6).

We hypothesized that perturbations to the H3 N-tail with H2A.Z were partially responsible for DNA unwrapping. By analyzing total contacts between the H3 N-tail and DNA, we found that the number of contacts was substantially lower with H2A.Z as compared to H2A (Figure 7E). Similarly, the number of contacts between the H2A.Z C-tail and DNA showed a significant decrease, consistent with a previous report (Figure 7E).[47] This is not surprising as the H2A.Z C-tail is shorter and contains fewer positively charged residues, making it less prone to interact with DNA. Closer inspection revealed that key hydrogen bonds between positively charged residues in the H3 N-tail (i.e. R17, R26, and R42) and the DNA backbone were disrupted in the H2A.Z system (Figure S12). We also observed multiple contacts between R42 and the H2A C-tail that would be missing with H2A.Z, including hydrogen bonds with the side chain and backbone carbonyl of E121 (Figure S13). This suggests the potential for an R42-E121 salt bridge, a strong interaction that has been visualized in the 1.9 Å resolution nucleosome structure (PDB ID:1KX5)[86] and further supported by our NMR data (Figure S8). Collectively, our findings support a model where H2A.Z incorporation disrupts key contacts between the H2A C-tail and H3 N-tail as well as DNA, leading to increased DNA accessibility that facilitates Sox2 and Oct4 engagement (Figure 6B).

Discussion

The histone variant H2A.Z can enhance chromatin accessibility and promote its interaction with chromatin factors to regulate gene expression. Here, we provide new molecular insights from experiments and computation that shed light on the role of H2A.Z in the interaction of pioneer factors Sox2 and Oct4 with nucleosomes. We find improved binding of Sox2 and Oct4 with H2A.Z at both end-positioned (SHL6) and internal (SHL2 for Sox2) nucleosome sites, which we correlate by NMR and simulation with more extensive DNA unwrapping and perturbed H3 N-tail conformational dynamics. Simultaneously, we demonstrate that Sox2 competes with and displaces the H3 N-tail when associating at the same nucleosome positions. Sox2 and Oct4 binding could be favored by higher DNA accessibility and mobility and lower competition with H3 tails. Thus, we show that pioneer factors can take advantage of H2A.Z-mediated changes in nucleosome conformation and dynamics to achieve more efficient

engagement with chromatin. Other destabilizing histone tail disease-linked mutations, epigenetic modifications or proteolytic clipping could have similar and potentially greater impact on pioneer factor-chromatin interactions. Our findings support an emerging mechanism where histone tails and their epigenetics alter nucleosome dynamics and recognition to tune chromatin function.[29, 30, 35, 38]

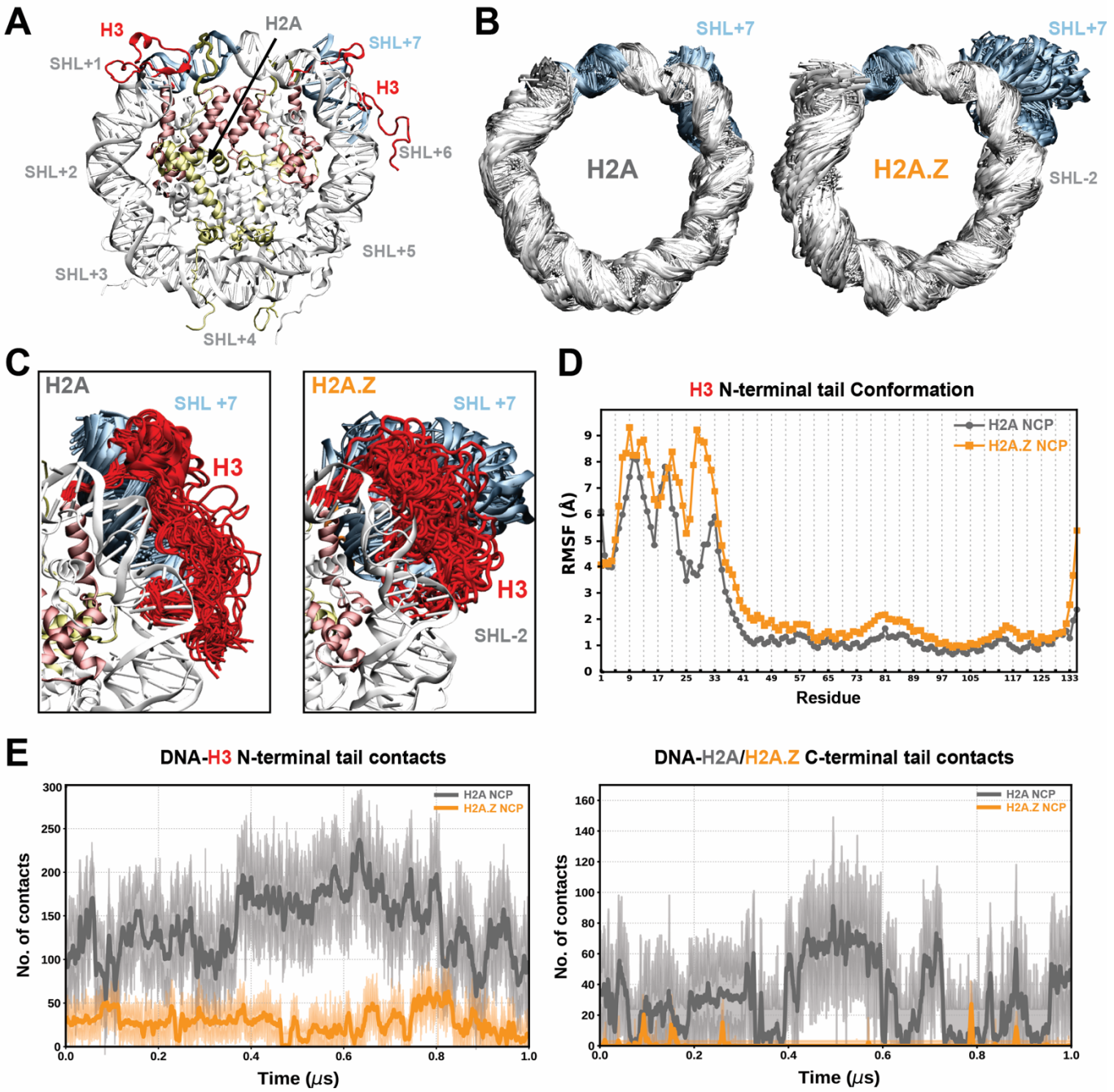

Figure 7. Increased DNA unwrapping is coupled to higher H3 fluctuations and fewer tail-DNA contacts in the presence of H2A.Z. (A) The modeled structure of NCP with superhelical locations (SHL+), highlighting H2A (yellow), H3 (red), and DNA at SHL+7 (ice blue, also denoting the dyad to SHL+1 for this DNA gyre). (B) The fluctuation of nucleosomal DNA in superimposed conformations for H2A (left) and H2A.Z (right) in the MD simulations, showing larger unwrapping and overall DNA mobility with H2A.Z. (C) Structural conformations of H3 N-terminal tails (red) during the MD simulations depicting higher disorder and altered conformations with H2A.Z, shifted away from SHL-2. (D) Root-mean-square fluctuations (RMSF) for Cα atoms of histone H3 for H2A (grey) and H2A.Z (orange) systems showing overall greater fluctuations with H2A.Z, especially in the H3 N-tail. (E) Number of contacts (4.5 Å cutoff) between the H3 N-tail (left) or the H2A/H2A.Z C-tail (right) and DNA as a function of time, showing fewer contacts in the H2A.Z system (orange) as compared to the H2A system (gray).

The destabilizing effect of H2A.Z on nucleosomes has been previously linked to its shorter and less positively charged C-terminal tail.[44, 45, 47] Prior computational studies have reported fewer overall and more transient contacts of the H2A.Z C-tail with DNA that correlate with greater unwrapping.[47] Moreover, deletion of the H2A C-tail also leads to increased histone exchange kinetics and nucleosome mobility *in vitro* and *in vivo*, implicating C-tail variants in similar functions.[39, 87] Our results corroborate these findings but also provide new important insights into the H3 N-tail and its role in DNA dynamics. We demonstrate that, with H2A.Z, the H3 N-tail is more disordered and adopts distinct conformations with fewer DNA contacts. H3 N-tail conformations that correlate with larger DNA unwrapping also bridge fewer contacts between the two DNA gyres and rarely interact with SHL2. These atomic detail insights are validated by the striking agreement we see between the differences in H3 fluctuations by simulation and the differences in H3 N-tail dynamics obtained by NMR for H2A.Z versus H2A systems. Importantly, the conformational changes in H3 result in better access to DNA at locations where we observe improved binding of Sox2 or Oct4 and where many other chromatin factors interact.[37, 38, 88]

Notably, our integrated NMR and MD data support a coupling between the H3 and H2A tail regions, which becomes impaired with H2A.Z. Our simulations show formation of a salt bridge between H3 R42 and H2A E121 that is supported by our NMR data and experimentally visualized once before.[86] By NMR, we observe a large change in E121 chemical shift, similar to an H2A-H2B dimer alone bound to DNA, in a destabilized H2A.Z$^{C\text{-}H2A}$ NCP that exhibits greater H3 N-tail dynamics and DNA unwrapping relative to the canonical NCP. The altered NMR signature could indicate disruption of the 3_{10}-helix observed in this region[86] and/or loss of C-tail contacts with H3 R42 or DNA. Additionally, we find that while Sox2 binding at SHL6 globally perturbs the H3 N-terminal tail for both H2A and H2A.Z nucleosomes, this has a noticeable effect only on the C-tail of H2A and not the mutant or variant C-tail, consistent with weakened H3 and DNA contacts there. We propose that this potential interaction between H2A E121 and H3 R42, absent with H2A.Z, could play a pivotal role in stabilizing the H3 and H2A tails at entry/exit DNA to prevent unwrapping. H3 R42 can alternatively make hydrogen bonds with the DNA backbone.[30, 89] Importantly, methylation at that site that would abolish H2A or DNA interactions has been shown to stimulate transcription *in vitro*.[90] On the other hand, mutations of H2A E121 (i.e. E121Q/K) are frequently encountered in human cancers and have been linked to disruption of higher-order chromatin structure.[41] Further mutational studies of these and other tail residues could establish the significance of specific interactions on nucleosome structure and dynamics.

We also demonstrate that the effect of H2A.Z is dependent on DNA sequence and greater for less stable nucleosomes such as Lin28B. With H2A.Z, we find that Lin28B is more accessible or dynamic around the central dyad, which could result from the enhanced unwrapping or internal flexibility of DNA. This could affect chromatin recognition by a variety of proteins targeting the nucleosome dyad region.[37, 88] Moreover, we observe that the canonical Lin28B nucleosome is already less stable and more dynamic than any 601* construct and exhibits H3 N-tail conformations consistent with less DNA interaction. This large-scale increase in DNA mobility could explain the ability of Sox2 to associate at multiple Lin28B sites that do not match its canonical motif. We have previously shown,[59] and further validated here, that mutations that disrupt DNA contacts and increase DNA mobility at the nucleosome edge (SHL6, H3 R49A) or internally (SHL2, H3 R83A) also enhance Sox2 binding. With Lin28B, Sox2 appears to globally change the nucleosome conformation by inducing deformations or repositioning of DNA. This is consistent with prior studies showing that binding of Sox2 and Oct4 to nucleosomes is accompanied by large DNA distortions and can evict the linker histone H1 from nucleosomes,[57, 58, 61, 91] which can potentially disrupt local and higher-order chromatin packing. Moreover, H1 and H2A.Z seem to have opposing functions as the binding of H1 to nucleosomes is inhibited by the H2A.Z C-tail[92] and the activity of H1 in yeast rDNA can be counteracted by H2A.Z.[93] Thus, we speculate that more labile genomic nucleosomes, in combination with epigenetic marks, can enable interactions with

pioneer factors, leading to structural changes that promote more relaxed chromatin states and increase the potential for chromatin remodeling.

Finally, we establish that Sox2 can significantly perturb the histone tails of both canonical and variant nucleosomes. We find that Sox2 can displace the N-tail of H3 when associating with 601* and Lin28B nucleosomes at both internal and end positions (SHL2, 5, 6, and also SHL3 in Lin28B), with a larger effect in the presence of destabilizing H2A.Z and mutant histones. Moreover, Sox2 binding can visibly perturb the C- and N-tail of H2A (SHL6) as well as the N-tail of H2B (SHL5, to be published elsewhere). While the H4 N-tail was not significantly affected by Sox2 binding at SHL2, that might not be the case when other nucleosome positions are targeted. Collectively, our data illustrates that Sox2 can directly and allosterically disrupt the conformation and dynamics of multiple histone tails known to regulate DNA dynamics, histone octamer interactions, and nucleosome sliding.[33, 34, 39, 94-96] Perturbations to histone tails by pioneer factors could have a major impact on chromatin structure, recognition, and epigenetic changes. Future research efforts should explore the role of these and other pioneer factors on histone tail conformation and dynamics, and how that might propagate to higher-order chromatin structure or tune the activity of chromatin readers and writers.

Acknowledgements

We thank Prof. Gregory Bowman (JHU) for kindly providing materials and access to instrumentation and Prof. Carl Wu (JHU) for the H2A.Z plasmid. We acknowledge Fabiana Malaga Gadea for preparing protein and nucleosome samples. We are grateful to Dr. Ananya Majumdar, director of the Biomolecular NMR center (JHU), for assistance with NMR data collection and to the Integrated Imaging Center (JHU) staff for bioimager training and support. This research was supported by grants R01GM147642 awarded to E.N.N. and 1R15GM146228 awarded to S.M.L. R. P. is grateful for support from The Rosemary O'Halloran Scholarship.

Supplementary Data

Supplementary Data are available at NAR online.

Data Availability

Analysis codes are available on GitHub Repository https://github.com/CUNY-CSI-Loverde-Laboratory/H2A.Z_Variant_MD_Analysis. Simulation trajectories will be made available on Zenodo. NMR chemical shift perturbation data for histone tails have been deposited to the Biological Magnetic Resonance Bank (BMRB IDs: 52922-52935).

Competing Interests

The authors declare no competing interests.

References

(1) Bannister, A. J.; Kouzarides, T. Regulation of chromatin by histone modifications. *Cell Res* **2011**, *21* (3), 381-395. DOI: 10.1038/cr.2011.22.
(2) Martire, S.; Banaszynski, L. A. The roles of histone variants in fine-tuning chromatin organization and function. *Nat Rev Mol Cell Biol* **2020**, *21* (9), 522-541. DOI: 10.1038/s41580-020-0262-8.
(3) Guillemette, B.; Gaudreau, L. Reuniting the contrasting functions of H2A.Z. *Biochem Cell Biol* **2006**, *84* (4), 528-535. DOI: 10.1139/o06-077.
(4) Giaimo, B. D.; Ferrante, F.; Herchenrother, A.; Hake, S. B.; Borggrefe, T. The histone variant H2A.Z in gene regulation. *Epigenetics Chromatin* **2019**, *12* (1), 37. DOI: 10.1186/s13072-019-0274-9.
(5) Colino-Sanguino, Y.; Clark, S. J.; Valdes-Mora, F. The H2A.Z-nucleosome code in mammals: emerging functions. *Trends Genet* **2022**, *38* (3), 273-289. DOI: 10.1016/j.tig.2021.10.003.
(6) Yin, X. M.; Zeng, D.; Liao, Y. J.; Tang, C. Y.; Li, Y. The Function of H2A Histone Variants and Their Roles in Diseases. *Biomolecules* **2024**, *14* (8). DOI: ARTN 993
10.3390/biom14080993.
(7) Hu, G.; Cui, K.; Northrup, D.; Liu, C.; Wang, C.; Tang, Q.; Ge, K.; Levens, D.; Crane-Robinson, C.; Zhao, K. H2A.Z facilitates access of active and repressive complexes to chromatin in embryonic stem cell self-renewal and differentiation. *Cell Stem Cell* **2013**, *12* (2), 180-192. DOI: 10.1016/j.stem.2012.11.003.
(8) Lai, P. M.; Chan, K. M. Roles of Histone H2A Variants in Cancer Development, Prognosis, and Treatment. *Int J Mol Sci* **2024**, *25* (6). DOI: 10.3390/ijms25063144.
(9) Raisner, R. M.; Hartley, P. D.; Meneghini, M. D.; Bao, M. Z.; Liu, C. L.; Schreiber, S. L.; Rando, O. J.; Madhani, H. D. Histone variant H2A.Z marks the 5' ends of both active and inactive genes in euchromatin. *Cell* **2005**, *123* (2), 233-248. DOI: 10.1016/j.cell.2005.10.002.
(10) Guillemette, B.; Bataille, A. R.; Gevry, N.; Adam, M.; Blanchette, M.; Robert, F.; Gaudreau, L. Variant histone H2A.Z is globally localized to the promoters of inactive yeast genes and regulates nucleosome positioning. *PLoS Biol* **2005**, *3* (12), e384. DOI: 10.1371/journal.pbio.0030384.
(11) Li, B.; Pattenden, S. G.; Lee, D.; Gutierrez, J.; Chen, J.; Seidel, C.; Gerton, J.; Workman, J. L. Preferential occupancy of histone variant H2AZ at inactive promoters influences local histone modifications and chromatin remodeling. *Proc Natl Acad Sci U S A* **2005**, *102* (51), 18385-18390. DOI: 10.1073/pnas.0507975102.
(12) Dai, X.; Bai, Y.; Zhao, L.; Dou, X.; Liu, Y.; Wang, L.; Li, Y.; Li, W.; Hui, Y.; Huang, X.; et al. H2A.Z Represses Gene Expression by Modulating Promoter Nucleosome Structure and Enhancer Histone Modifications in Arabidopsis. *Mol Plant* **2017**, *10* (10), 1274-1292. DOI: 10.1016/j.molp.2017.09.007.
(13) Valdes-Mora, F.; Song, J. Z.; Statham, A. L.; Strbenac, D.; Robinson, M. D.; Nair, S. S.; Patterson, K. I.; Tremethick, D. J.; Stirzaker, C.; Clark, S. J. Acetylation of H2A.Z is a key epigenetic modification associated with gene deregulation and epigenetic remodeling in cancer. *Genome Res* **2012**, *22* (2), 307-321. DOI: 10.1101/gr.118919.110.
(14) Chen, J.; Miller, A.; Kirchmaier, A. L.; Irudayaraj, J. M. Single-molecule tools elucidate H2A.Z nucleosome composition. *J Cell Sci* **2012**, *125* (Pt 12), 2954-2964. DOI: 10.1242/jcs.101592.
(15) Reda, A.; Hategan, L. A.; McLean, T. A. B.; Creighton, S. D.; Luo, J. Q.; Chen, S. E. S.; Hua, S.; Winston, S.; Reeves, I.; Padmanabhan, A.; et al. Role of the histone variant H2A.Z.1 in memory, transcription, and alternative splicing is mediated by lysine modification. *Neuropsychopharmacology* **2024**, *49* (8), 1285-1295. DOI: 10.1038/s41386-024-01817-2.
(16) Jin, C.; Zang, C.; Wei, G.; Cui, K.; Peng, W.; Zhao, K.; Felsenfeld, G. H3.3/H2A.Z double variant-containing nucleosomes mark 'nucleosome-free regions' of active promoters and other regulatory regions. *Nat Genet* **2009**, *41* (8), 941-945. DOI: 10.1038/ng.409.
(17) Du, Y.; Liu, Z.; Cao, X.; Chen, X.; Chen, Z.; Zhang, X.; Zhang, X.; Jiang, C. Nucleosome eviction along with H3K9ac deposition enhances Sox2 binding during human neuroectodermal commitment. *Cell Death Differ* **2017**, *24* (6), 1121-1131. DOI: 10.1038/cdd.2017.62.

(18) Wen, Z.; Zhang, L.; Ruan, H.; Li, G. Histone variant H2A.Z regulates nucleosome unwrapping and CTCF binding in mouse ES cells. *Nucleic Acids Res* **2020**, *48* (11), 5939-5952. DOI: 10.1093/nar/gkaa360.
(19) Li, Z.; Gadue, P.; Chen, K.; Jiao, Y.; Tuteja, G.; Schug, J.; Li, W.; Kaestner, K. H. Foxa2 and H2A.Z mediate nucleosome depletion during embryonic stem cell differentiation. *Cell* **2012**, *151* (7), 1608-1616. DOI: 10.1016/j.cell.2012.11.018.
(20) Wang, J.; Qiao, M.; He, Q.; Shi, R.; Loh, S. J.; Stanton, L. W.; Wu, M. Pluripotency Activity of Nanog Requires Biochemical Stabilization by Variant Histone Protein H2A.Z. *Stem Cells* **2015**, *33* (7), 2126-2134. DOI: 10.1002/stem.2011.
(21) Cauchy, P.; Koch, F.; Andrau, J. C. Two possible modes of pioneering associated with combinations of H2A.Z and p300/CBP at nucleosome-occupied enhancers. *Transcription-Austin* **2017**, *8* (3), 179-184. DOI: 10.1080/21541264.2017.1291395.
(22) Sporrij, A.; Choudhuri, A.; Prasad, M.; Muhire, B.; Fast, E. M.; Manning, M. E.; Weiss, J. D.; Koh, M.; Yang, S.; Kingston, R. E.; et al. PGE2 alters chromatin through H2A.Z-variant enhancer nucleosome modification to promote hematopoietic stem cell fate. *Proceedings of the National Academy of Sciences of the United States of America* **2023**, *120* (19). DOI: ARTN e2220613120
10.1073/pnas.2220613120.
(23) Xu, J.; Watts, J. A.; Pope, S. D.; Gadue, P.; Kamps, M.; Plath, K.; Zaret, K. S.; Smale, S. T. Transcriptional competence and the active marking of tissue-specific enhancers by defined transcription factors in embryonic and induced pluripotent stem cells. *Genes Dev* **2009**, *23* (24), 2824-2838. DOI: 10.1101/gad.1861209.
(24) Iwafuchi-Doi, M.; Zaret, K. S. Cell fate control by pioneer transcription factors. *Development* **2016**, *143* (11), 1833-1837. DOI: 10.1242/dev.133900.
(25) Zhou, C.; Yang, X.; Sun, Y.; Yu, H.; Zhang, Y.; Jin, Y. Comprehensive profiling reveals mechanisms of SOX2-mediated cell fate specification in human ESCs and NPCs. *Cell Res* **2016**, *26* (2), 171-189. DOI: 10.1038/cr.2016.15.
(26) Halblander, F. N.; Meng, F. W.; Murphy, P. J. Anp32e protects against accumulation of H2A.Z at Sox motif containing promoters during zebrafish gastrulation. *Developmental Biology* **2024**, *507*, 34-43. DOI: 10.1016/j.ydbio.2023.12.010.
(27) Anderson, J. D.; Lowary, P. T.; Widom, J. Effects of histone acetylation on the equilibrium accessibility of nucleosomal DNA target sites. *J Mol Biol* **2001**, *307* (4), 977-985. DOI: 10.1006/jmbi.2001.4528
S0022-2836(01)94528-0 [pii].
(28) Tims, H. S.; Gurunathan, K.; Levitus, M.; Widom, J. Dynamics of nucleosome invasion by DNA binding proteins. *J Mol Biol* **2011**, *411* (2), 430-448. DOI: 10.1016/j.jmb.2011.05.044.
(29) Peng, Y. H.; Li, S. X.; Onufriev, A.; Landsman, D.; Panchenko, A. R. Binding of regulatory proteins to nucleosomes is modulated by dynamic histone tails. *Nature Communications* **2021**, *12* (1). DOI: ARTN 5280
10.1038/s41467-021-25568-6.
(30) Armeev, G. A.; Kniazeva, A. S.; Komarova, G. A.; Kirpichnikov, M. P.; Shaytan, A. K. Histone dynamics mediate DNA unwrapping and sliding in nucleosomes. *Nat Commun* **2021**, *12* (1), 2387. DOI: 10.1038/s41467-021-22636-9.
(31) Khatua, P.; Tang, P. K.; Ghosh Moulick, A.; Patel, R.; Manandhar, A.; Loverde, S. M. Sequence Dependence in Nucleosome Dynamics. *J Phys Chem B* **2024**, *128* (13), 3090-3101. DOI: 10.1021/acs.jpcb.3c07363.
(32) Gao, M.; Nadaud, P. S.; Bernier, M. W.; North, J. A.; Hammel, P. C.; Poirier, M. G.; Jaroniec, C. P. Histone H3 and H4 N-Terminal Tails in Nucleosome Arrays at Cellular Concentrations Probed by Magic Angle Spinning NMR Spectroscopy. *Journal of the American Chemical Society* **2013**, *135* (41), 15278-15281. DOI: 10.1021/ja407526s.

(33) Erler, J.; Zhang, R.; Petridis, L.; Cheng, X.; Smith, J. C.; Langowski, J. The role of histone tails in the nucleosome: a computational study. *Biophys J* **2014**, *107* (12), 2911-2922. DOI: 10.1016/j.bpj.2014.10.065.
(34) Chakraborty, K.; Loverde, S. M. Asymmetric breathing motions of nucleosomal DNA and the role of histone tails. *J Chem Phys* **2017**, *147* (6), 065101. DOI: 10.1063/1.4997573.
(35) Morrison, E. A.; Bowerman, S.; Sylvers, K. L.; Wereszczynski, J.; Musselman, C. A. The conformation of the histone H3 tail inhibits association of the BPTF PHD finger with the nucleosome. *Elife* **2018**, *7*. DOI: 10.7554/eLife.31481.
(36) Zhu, F.; Farnung, L.; Kaasinen, E.; Sahu, B.; Yin, Y.; Wei, B.; Dodonova, S. O.; Nitta, K. R.; Morgunova, E.; Taipale, M.; et al. The interaction landscape between transcription factors and the nucleosome. *Nature* **2018**, *562* (7725), 76-81. DOI: 10.1038/s41586-018-0549-5.
(37) Morgunova, E.; Taipale, J. Structural insights into the interaction between transcription factors and the nucleosome. *Current Opinion in Structural Biology* **2021**, *71*, 171-179. DOI: 10.1016/j.sbi.2021.06.016.
(38) Orsetti, A.; van Oosten, D.; Vasarhelyi, R. G.; Danescu, T. M.; Huertas, J.; van Ingen, H.; Cojocaru, V. Structural dynamics in chromatin unraveling by pioneer transcription factors. *Biophys Rev* **2024**, *16* (3), 365-382. DOI: 10.1007/s12551-024-01205-6.
(39) Biswas, M.; Voltz, K.; Smith, J. C.; Langowski, J. Role of histone tails in structural stability of the nucleosome. *PLoS Comput Biol* **2011**, *7* (12), e1002279. DOI: 10.1371/journal.pcbi.1002279.
(40) Azad, G. K.; Swagatika, S.; Kumawat, M.; Kumawat, R.; Tomar, R. S. Modifying Chromatin by Histone Tail Clipping. *J Mol Biol* **2018**, *430* (18 Pt B), 3051-3067. DOI: 10.1016/j.jmb.2018.07.013.
(41) Espinoza Pereira, K. N.; Shan, J.; Licht, J. D.; Bennett, R. L. Histone mutations in cancer. *Biochem Soc Trans* **2023**, *51* (5), 1749-1763. DOI: 10.1042/BST20210567.
(42) Fenley, A. T.; Anandakrishnan, R.; Kidane, Y. H.; Onufriev, A. V. Modulation of nucleosomal DNA accessibility via charge-altering post-translational modifications in histone core. *Epigenetics Chromatin* **2018**, *11* (1), 11. DOI: 10.1186/s13072-018-0181-5.
(43) Horikoshi, N.; Arimura, Y.; Taguchi, H.; Kurumizaka, H. Crystal structures of heterotypic nucleosomes containing histones H2A.Z and H2A. *Open Biol* **2016**, *6* (6). DOI: 10.1098/rsob.160127.
(44) Lewis, T. S.; Sokolova, V.; Jung, H.; Ng, H.; Tan, D. Structural basis of chromatin regulation by histone variant H2A.Z. *Nucleic Acids Res* **2021**, *49* (19), 11379-11391. DOI: 10.1093/nar/gkab907.
(45) Sato, S.; Tanaka, N.; Arimura, Y.; Kujirai, T.; Kurumizaka, H. The N-terminal and C-terminal halves of histone H2A.Z independently function in nucleosome positioning and stability. *Genes Cells* **2020**, *25* (8), 538-546. DOI: 10.1111/gtc.12791.
(46) Bowerman, S.; Wereszczynski, J. Effects of MacroH2A and H2A.Z on Nucleosome Dynamics as Elucidated by Molecular Dynamics Simulations. *Biophysical Journal* **2016**, *110* (2), 327-337. DOI: 10.1016/j.bpj.2015.12.015.
(47) Li, S.; Wei, T.; Panchenko, A. R. Histone variant H2A.Z modulates nucleosome dynamics to promote DNA accessibility. *Nat Commun* **2023**, *14* (1), 769. DOI: 10.1038/s41467-023-36465-5.
(48) Kashyap, V.; Rezende, N. C.; Scotland, K. B.; Shaffer, S. M.; Persson, J. L.; Gudas, L. J.; Mongan, N. P. Regulation of stem cell pluripotency and differentiation involves a mutual regulatory circuit of the NANOG, OCT4, and SOX2 pluripotency transcription factors with polycomb repressive complexes and stem cell microRNAs. *Stem Cells Dev* **2009**, *18* (7), 1093-1108. DOI: 10.1089/scd.2009.0113.
(49) Wang, J.; Rao, S.; Chu, J.; Shen, X.; Levasseur, D. N.; Theunissen, T. W.; Orkin, S. H. A protein interaction network for pluripotency of embryonic stem cells. *Nature* **2006**, *444* (7117), 364-368. DOI: 10.1038/nature05284.
(50) Iwafuchi-Doi, M.; Zaret, K. S. Pioneer transcription factors in cell reprogramming. *Genes Dev* **2014**, *28* (24), 2679-2692. DOI: 10.1101/gad.253443.114.
(51) Rodda, D. J.; Chew, J. L.; Lim, L. H.; Loh, Y. H.; Wang, B.; Ng, H. H.; Robson, P. Transcriptional regulation of nanog by OCT4 and SOX2. *J Biol Chem* **2005**, *280* (26), 24731-24737. DOI: 10.1074/jbc.M502573200.

(52) Li, S.; Zheng, E. B.; Zhao, L.; Liu, S. Nonreciprocal and Conditional Cooperativity Directs the Pioneer Activity of Pluripotency Transcription Factors. *Cell Rep* **2019**, *28* (10), 2689-2703 e2684. DOI: 10.1016/j.celrep.2019.07.103.
(53) Chen, X.; Xu, H.; Yuan, P.; Fang, F.; Huss, M.; Vega, V. B.; Wong, E.; Orlov, Y. L.; Zhang, W.; Jiang, J.; et al. Integration of external signaling pathways with the core transcriptional network in embryonic stem cells. *Cell* **2008**, *133* (6), 1106-1117. DOI: 10.1016/j.cell.2008.04.043.
(54) Remenyi, A.; Lins, K.; Nissen, L. J.; Reinbold, R.; Scholer, H. R.; Wilmanns, M. Crystal structure of a POU/HMG/DNA ternary complex suggests differential assembly of Oct4 and Sox2 on two enhancers. *Genes Dev* **2003**, *17* (16), 2048-2059. DOI: 10.1101/gad.269303.
(55) Williams, D. C., Jr.; Cai, M.; Clore, G. M. Molecular basis for synergistic transcriptional activation by Oct1 and Sox2 revealed from the solution structure of the 42-kDa Oct1.Sox2.Hoxb1-DNA ternary transcription factor complex. *J Biol Chem* **2004**, *279* (2), 1449-1457. DOI: 10.1074/jbc.M309790200.
(56) Soufi, A.; Garcia, M. F.; Jaroszewicz, A.; Osman, N.; Pellegrini, M.; Zaret, K. S. Pioneer transcription factors target partial DNA motifs on nucleosomes to initiate reprogramming. *Cell* **2015**, *161* (3), 555-568. DOI: 10.1016/j.cell.2015.03.017.
(57) Dodonova, S. O.; Zhu, F.; Dienemann, C.; Taipale, J.; Cramer, P. Nucleosome-bound SOX2 and SOX11 structures elucidate pioneer factor function. *Nature* **2020**, *580* (7805), 669-672. DOI: 10.1038/s41586-020-2195-y.
(58) Michael, A. K.; Grand, R. S.; Isbel, L.; Cavadini, S.; Kozicka, Z.; Kempf, G.; Bunker, R. D.; Schenk, A. D.; Graff-Meyer, A.; Pathare, G. R.; et al. Mechanisms of OCT4-SOX2 motif readout on nucleosomes. *Science* **2020**, *368* (6498), 1460-1465. DOI: 10.1126/science.abb0074.
(59) Malaga Gadea, F. C.; Nikolova, E. N. Structural Plasticity of Pioneer Factor Sox2 and DNA Bendability Modulate Nucleosome Engagement and Sox2-Oct4 Synergism. *J Mol Biol* **2023**, *435* (2), 167916. DOI: 10.1016/j.jmb.2022.167916.
(60) MacCarthy, C. M.; Huertas, J.; Ortmeier, C.; Vom Bruch, H.; Tan, D. S.; Reinke, D.; Sander, A.; Bergbrede, T.; Jauch, R.; Scholer, H. R.; et al. OCT4 interprets and enhances nucleosome flexibility. *Nucleic Acids Res* **2022**, *50* (18), 10311-10327. DOI: 10.1093/nar/gkac755.
(61) Guan, R.; Lian, T.; Zhou, B. R.; Wheeler, D.; Bai, Y. Structural mechanism of LIN28B nucleosome targeting by OCT4. *Mol Cell* **2023**, *83* (12), 1970-1982 e1976. DOI: 10.1016/j.molcel.2023.05.030.
(62) Sinha, K. K.; Bilokapic, S.; Du, Y.; Malik, D.; Halic, M. Histone modifications regulate pioneer transcription factor cooperativity. *Nature* **2023**, *619* (7969), 378-384. DOI: 10.1038/s41586-023-06112-6.
(63) Luger, K.; Rechsteiner, T. J.; Richmond, T. J. Preparation of nucleosome core particle from recombinant histones. *Methods Enzymol* **1999**, *304*, 3-19.
(64) Nodelman, I. M.; Patel, A.; Levendosky, R. F.; Bowman, G. D. Reconstitution and Purification of Nucleosomes with Recombinant Histones and Purified DNA. *Curr Protoc Mol Biol* **2020**, *133* (1), e130. DOI: 10.1002/cpmb.130.
(65) Rueden, C. T.; Schindelin, J.; Hiner, M. C.; DeZonia, B. E.; Walter, A. E.; Arena, E. T.; Eliceiri, K. W. ImageJ2: ImageJ for the next generation of scientific image data. *BMC Bioinformatics* **2017**, *18* (1), 529. DOI: 10.1186/s12859-017-1934-z.
(66) Delaglio, F.; Grzesiek, S.; Vuister, G. W.; Zhu, G.; Pfeifer, J.; Bax, A. NMRPipe: a multidimensional spectral processing system based on UNIX pipes. *J Biomol NMR* **1995**, *6* (3), 277-293.
(67) Vasudevan, D.; Chua, E. Y. D.; Davey, C. A. Crystal structures of nucleosome core particles containing the '601' strong positioning sequence. *J Mol Biol* **2010**, *403* (1), 1-10. DOI: 10.1016/j.jmb.2010.08.039.
(68) Goddard, T. D.; Huang, C. C.; Meng, E. C.; Pettersen, E. F.; Couch, G. S.; Morris, J. H.; Ferrin, T. E. UCSF ChimeraX: Meeting modern challenges in visualization and analysis. *Protein Sci* **2018**, *27* (1), 14-25. DOI: 10.1002/pro.3235.
(69) Suto, R. K.; Clarkson, M. J.; Tremethick, D. J.; Luger, K. Crystal structure of a nucleosome core particle containing the variant histone H2A.Z. *Nat Struct Biol* **2000**, *7* (12), 1121-1124. DOI: 10.1038/81971.

(70) Humphrey, W.; Dalke, A.; Schulten, K. VMD: visual molecular dynamics. *Journal of molecular graphics* **1996**, *14* (1), 33-38, 27-38, Research Support, Non-U.S. Gov't
Research Support, U.S. Gov't, Non-P.H.S.
Research Support, U.S. Gov't, P.H.S.
(71) Tian, C.; Kasavajhala, K.; Belfon, K. A. A.; Raguette, L.; Huang, H.; Migues, A. N.; Bickel, J.; Wang, Y.; Pincay, J.; Wu, Q.; et al. ff19SB: Amino-Acid-Specific Protein Backbone Parameters Trained against Quantum Mechanics Energy Surfaces in Solution. *J Chem Theory Comput* **2020**, *16* (1), 528-552. DOI: 10.1021/acs.jctc.9b00591.
(72) Galindo-Murillo, R.; Robertson, J. C.; Zgarbova, M.; Sponer, J.; Otyepka, M.; Jurecka, P.; Cheatham, T. E., 3rd. Assessing the Current State of Amber Force Field Modifications for DNA. *J Chem Theory Comput* **2016**, *12* (8), 4114-4127. DOI: 10.1021/acs.jctc.6b00186.
(73) Khasawinah, K.; Alzoubi, Z.; Obeidat, A. Free-energy differences of OPC-water and SPC/HW-heavy-water models using the Bennett acceptance ratio. *Heliyon* **2022**, *8* (8), e10000. DOI: 10.1016/j.heliyon.2022.e10000.
(74) Kulkarni, M.; Yang, C.; Pak, Y. Refined Alkali Metal Ion Parameters for the OPC Water Model. *Bulletin of the Korean Chemical Society* **2018**, *39* (8), 931-935. DOI: 10.1002/bkcs.11527.
(75) Joung, I. S.; Cheatham, T. E., 3rd. Determination of alkali and halide monovalent ion parameters for use in explicitly solvated biomolecular simulations. *J Phys Chem B* **2008**, *112* (30), 9020-9041. DOI: 10.1021/jp8001614.
(76) Li, Z.; Song, L. F.; Li, P.; Merz, K. M., Jr. Systematic Parametrization of Divalent Metal Ions for the OPC3, OPC, TIP3P-FB, and TIP4P-FB Water Models. *J Chem Theory Comput* **2020**, *16* (7), 4429-4442. DOI: 10.1021/acs.jctc.0c00194.
(77) Lee, T. S.; Cerutti, D. S.; Mermelstein, D.; Lin, C.; LeGrand, S.; Giese, T. J.; Roitberg, A.; Case, D. A.; Walker, R. C.; York, D. M. GPU-Accelerated Molecular Dynamics and Free Energy Methods in Amber18: Performance Enhancements and New Features. *J Chem Inf Model* **2018**, *58* (10), 2043-2050. DOI: 10.1021/acs.jcim.8b00462.
(78) Van Der Spoel, D.; Lindahl, E.; Hess, B.; Groenhof, G.; Mark, A. E.; Berendsen, H. J. GROMACS: fast, flexible, and free. *J Comput Chem* **2005**, *26* (16), 1701-1718. DOI: 10.1002/jcc.20291.
(79) Yuan, H.; Corbi, N.; Basilico, C.; Dailey, L. Developmental-specific activity of the FGF-4 enhancer requires the synergistic action of Sox2 and Oct-3. *Genes Dev* **1995**, *9* (21), 2635-2645.
(80) Park, Y. J.; Dyer, P. N.; Tremethick, D. J.; Luger, K. A new fluorescence resonance energy transfer approach demonstrates that the histone variant H2AZ stabilizes the histone octamer within the nucleosome. *Journal of Biological Chemistry* **2004**, *279* (23), 24274-24282. DOI: 10.1074/jbc.M313152200.
(81) Huertas, J.; MacCarthy, C. M.; Scholer, H. R.; Cojocaru, V. Nucleosomal DNA Dynamics Mediate Oct4 Pioneer Factor Binding. *Biophys J* **2020**, *118* (9), 2280-2296. DOI: 10.1016/j.bpj.2019.12.038.
(82) Zhou, B. R.; Feng, H.; Ghirlando, R.; Kato, H.; Gruschus, J.; Bai, Y. Histone H4 K16Q mutation, an acetylation mimic, causes structural disorder of its N-terminal basic patch in the nucleosome. *J Mol Biol* **2012**, *421* (1), 30-37. DOI: 10.1016/j.jmb.2012.04.032.
(83) Jennings, C. E.; Zoss, C. J.; Morrison, E. A. Arginine anchor points govern H3 tail dynamics. *Front Mol Biosci* **2023**, *10*, 1150400. DOI: 10.3389/fmolb.2023.1150400.
(84) Abramov, G.; Velyvis, A.; Rennella, E.; Wong, L. E.; Kay, L. E. A methyl-TROSY approach for NMR studies of high-molecular-weight DNA with application to the nucleosome core particle. *Proc Natl Acad Sci U S A* **2020**, *117* (23), 12836-12846. DOI: 10.1073/pnas.2004317117.
(85) Ohtomo, H.; Kurita, J. I.; Sakuraba, S.; Li, Z.; Arimura, Y.; Wakamori, M.; Tsunaka, Y.; Umehara, T.; Kurumizaka, H.; Kono, H.; et al. The N-terminal Tails of Histones H2A and H2B Adopt Two Distinct Conformations in the Nucleosome with Contact and Reduced Contact to DNA. *J Mol Biol* **2021**, *433* (15), 167110. DOI: 10.1016/j.jmb.2021.167110.
(86) Davey, C. A.; Sargent, D. F.; Luger, K.; Maeder, A. W.; Richmond, T. J. Solvent mediated interactions in the structure of the nucleosome core particle at 1.9 Å resolution. *Journal of Molecular Biology* **2002**, *319* (5), 1097-1113. DOI: 10.1016/S0022-2836(02)00386-8.

(87) Vogler, C.; Huber, C.; Waldmann, T.; Ettig, R.; Braun, L.; Izzo, A.; Daujat, S.; Chassignet, I.; Lopez-Contreras, A. J.; Fernandez-Capetillo, O.; et al. Histone H2A C-terminus regulates chromatin dynamics, remodeling, and histone H1 binding. *PLoS Genet* **2010**, *6* (12), e1001234. DOI: 10.1371/journal.pgen.1001234.
(88) Armeev, G. A.; Gribkova, A. K.; Shaytan, A. K. Nucleosomes and their complexes in the cryoEM era: Trends and limitations. *Front Mol Biosci* **2022**, *9*, 1070489. DOI: 10.3389/fmolb.2022.1070489.
(89) Shi, X.; Prasanna, C.; Soman, A.; Pervushin, K.; Nordenskiold, L. Dynamic networks observed in the nucleosome core particles couple the histone globular domains with DNA. *Commun Biol* **2020**, *3* (1), 639. DOI: 10.1038/s42003-020-01369-3.
(90) Casadio, F.; Lu, X.; Pollock, S. B.; LeRoy, G.; Garcia, B. A.; Muir, T. W.; Roeder, R. G.; Allis, C. D. H3R42me2a is a histone modification with positive transcriptional effects. *Proc Natl Acad Sci U S A* **2013**, *110* (37), 14894-14899. DOI: 10.1073/pnas.1312925110.
(91) Echigoya, K.; Koyama, M.; Negishi, L.; Takizawa, Y.; Mizukami, Y.; Shimabayashi, H.; Kuroda, A.; Kurumizaka, H. Nucleosome binding by the pioneer transcription factor OCT4. *Sci Rep* **2020**, *10* (1), 11832. DOI: 10.1038/s41598-020-68850-1.
(92) Lazarovici, A.; Zhou, T.; Shafer, A.; Dantas Machado, A. C.; Riley, T. R.; Sandstrom, R.; Sabo, P. J.; Lu, Y.; Rohs, R.; Stamatoyannopoulos, J. A.; et al. Probing DNA shape and methylation state on a genomic scale with DNase I. *Proc Natl Acad Sci U S A* **2013**, *110* (16), 6376-6381. DOI: 10.1073/pnas.1216822110.
(93) Rogers, A. M.; Neri, N. R.; Chigweshe, L.; Holmes, S. G. Histone variant H2A.Z and linker histone H1 influence chromosome condensation in Saccharomyces cerevisiae. *Genetics* **2024**, *226* (4). DOI: 10.1093/genetics/iyae022.
(94) Hamiche, A.; Kang, J. G.; Dennis, C.; Xiao, H.; Wu, C. Histone tails modulate nucleosome mobility and regulate ATP-dependent nucleosome sliding by NURF. *Proc Natl Acad Sci U S A* **2001**, *98* (25), 14316-14321. DOI: 10.1073/pnas.251421398.
(95) Ferreira, H.; Somers, J.; Webster, R.; Flaus, A.; Owen-Hughes, T. Histone tails and the H3 alphaN helix regulate nucleosome mobility and stability. *Mol Cell Biol* **2007**, *27* (11), 4037-4048. DOI: 10.1128/MCB.02229-06.
(96) Bendandi, A.; Patelli, A. S.; Diaspro, A.; Rocchia, W. The role of histone tails in nucleosome stability: An electrostatic perspective. *Comput Struct Biotechnol J* **2020**, *18*, 2799-2809. DOI: 10.1016/j.csbj.2020.09.034.